

1 **The Derived-Band Envelope Following Response and its Sensi-**
2 **tivity to Sensorineural Hearing Deficits**

3
4 **Sarineh Keshishzadeh***

5 Hearing Technology @ WAVES, Department of Information Technology, Ghent
6 University

7 Technologiepark 126, Zwijnaarde 9052, Belgium

8 *corresponding author: sarineh.keshishzadeh@ugent.be

9
10 **Markus Garrett**

11 Medizinische Physik and Cluster of Excellence Hearing4all, Department of
12 Medical Physics and Acoustics, University of Oldenburg

13 Carl-von-Ossietzky strasse 9-11, 26120 Oldenburg, Germany

14 Email: markus.garrett@uni-oldenburg.de

15
16 **Sarah Verhulst**

17 Hearing Technology @ WAVES, Department of Information Technology, Ghent
18 University

19 Technologiepark 126, Zwijnaarde 9052, Belgium

20 Email: s.verhulst@ugent.be

21
22 **Abstract**

23 The envelope following response (EFR) is a sensitive marker of synap-
24 topathy in animal models. However, its amplitude is affected by the spread

25 of basilar-membrane excitation and other coexisting sensorineural hearing
26 deficits. This study aims to (i) improve frequency specificity of the EFR
27 by introducing a derived-band EFR (DBEFR) technique and (ii) investigate
28 the effect of lifetime noise exposure, age and outer-hair-cell (OHC) damage
29 on DBEFR magnitudes. Additionally, we adopt a modelling approach to
30 validate the frequency-specificity of the DBEFR and test how different as-
31 pects of sensorineural hearing loss affect peripheral generators. The combined
32 analysis of simulations and experimental data proposes that the DBEFRs ex-
33 tracted from the [2-6]-kHz frequency band is a sensitive and frequency-specific
34 measure of synaptopathy in humans. Individual variability in DBEFR mag-
35 nitudes among listeners with normal audiograms was explained by their self-
36 reported amount of experienced lifetime noise-exposure and corresponded to
37 amplitude variability predicted by synaptopathy. Older listeners consistently
38 had reduced DBEFR amplitudes in comparison to young normal-hearing lis-
39 teners, in correspondence to how age-induced synaptopathy affects EFRs
40 and compromises temporal envelope encoding. Lastly, OHC damage was
41 also seen to affect the DBEFR amplitude, hence this marker should be com-
42 bined with a marker sensitive to OHC-damage to offer a differential diagnosis
43 of synaptopathy in listeners with impaired audiograms.

44 **Keywords**

45 derived-band envelope following response; cochlear synaptopathy; sen-
46 sorieneural hearing-loss; supra-threshold hearing deficits

47 **1. Introduction**

48 Struggling to understand speech in noisy environments is a prevalent
49 complaint of the ageing population, even if they have normal audiometric
50 thresholds. Although thresholds are informative about the sensory func-
51 tion of the cochlea, they are insensitive to auditory-nerve (AN) fiber loss,
52 which is the first sign of permanent hearing damage (Kujawa and Liberman,
53 2009; Liberman and Kujawa, 2017) and related to supra-threshold hearing
54 (Bharadwaj et al., 2014). Recent animal studies have shown that overex-
55 posure to noise, ageing and ototoxicity can lead to an irreversible loss of
56 AN synapses, i.e. cochlear synaptopathy (CS), and delayed degeneration of
57 cochlear neurons, while leaving the cochlear sensory hair cells intact (Kujawa
58 and Liberman, 2009; Lin et al., 2011; Liu et al., 2012; Furman et al., 2013;
59 Lobarinas et al., 2017; Valero et al., 2017). Even if the noise exposure dose
60 only causes a temporary threshold shift (Kujawa and Liberman, 2009), noise-
61 induced AN fibers degeneration can progress through the lifespan and yield
62 an increased sensitivity of the ear to age-induced hearing dysfunction (Fer-
63 nandez et al., 2015). Additionally, reduced numbers of spiral ganglion cells
64 in post-mortem histology of human temporal bones with preserved sensory
65 cells, confirmed the existence of age-related CS in humans (Makary et al.,
66 2011; Viana et al., 2015; Wu et al., 2019). Thus, noise exposure and ageing
67 are important causes of CS, a deficit which compromises the temporal coding
68 fidelity of supra-threshold sound as a result of a reduced number of afferent
69 AN synapses innervating the inner hair cell (Bharadwaj et al., 2014, 2015).

70 Since the discovery of CS, several attempts have been made to associate
71 changes in indirect and non-invasive measures of auditory function such as

72 scalp-recorded auditory evoked potentials (AEPs) to the histologically quan-
73 tified degree of AN fibers loss in animals. For example, auditory brainstem re-
74 sponses (ABRs), evoked by transient stimuli and reflecting the synchronized
75 onset responses of AN fibers (Don and Eggermont, 1978) showed a decreased
76 wave-I amplitude after synaptopathy due to noise-exposure (Kujawa and
77 Liberman, 2009; Lobarinas et al., 2017; Lin et al., 2011), despite recovered
78 normal distortion product otoacoustic emission (DPOAE) and ABR thresh-
79 olds. The number of AN fibers can also be quantified using envelope following
80 responses (EFRs), which capture how well AN fibers can phase-lock to the
81 stimulus envelope (Joris and Yin, 1992). The EFR can be extracted from
82 scalp-electrodes in response to a sinusoidally amplitude modulated (SAM)
83 pure-tone stimulus (Bharadwaj et al., 2014), and has been proposed as an
84 AEP-based measure of CS (Shaheen et al., 2015; Parthasarathy and Kujawa,
85 2018).

86 Despite the strong relation between AEP markers and CS in animal studies,
87 the indirect nature of AEP recordings hinders a clear and direct interpreta-
88 tion of response strength in terms of CS. First of all, a mixture of sources
89 contribute to scalp potentials, some of which are electrical activity induced by
90 subject-specific factors and unrelated to the sound-driven response (e.g. head
91 size, age, sex, geometry of the generators and physiological noise level, Trune
92 et al., 1988; Mitchell et al., 1989; Bharadwaj et al., 2014; Plack et al., 2016).
93 Other sources relate to the sound-driven response but depend on outer-hair-
94 cell (OHC) health (Gorga et al., 1985) or cochlear tonotopy (Don and Egger-
95 mont, 1978). Lastly, the scalp-recorded AEP is strongly influenced by stim-
96 ulus characteristics and the corresponding spread of basilar-membrane (BM)

97 excitation, which can confound a frequency-specific diagnosis of CS (Bharad-
98 waj et al., 2014, 2015; Verhulst et al., 2018a; Encina-Llamas et al., 2019). To
99 address these issues, several studies have proposed differential/relative AEP-
100 based metrics: the EFR amplitude slope as a function of modulation depth
101 (Bharadwaj et al., 2014, 2015), ABR wave-V latency changes in different
102 levels of background noise (Mehraei et al., 2016), EFR magnitude differences
103 to stimuli with different modulation depths (Bharadwaj et al., 2015; Guest
104 et al., 2018), or the combined use of EFR signal-to-noise ratios (SNRs) with
105 ABRs to segregate mixed hearing pathologies and normalize inter-individual
106 variabilities (Vasilkov and Verhulst, 2019). Secondly, a number of techniques
107 have been proposed to confine ABR generation to specific frequency bands:
108 the use of simultaneous off-frequency masking paradigms, i.e. the derived-
109 band ABR (Eggermont, 1976; Don and Eggermont, 1978), tone-burst ABRs
110 (Rasetshwane et al., 2013) and notched noise paradigms (Abdala and Fol-
111 som, 1995). Lastly, asynchrony of low-spontaneous rate (LSR) AN fibers to
112 the transient stimulus (Bourien et al., 2014) may limit the use of the ABR
113 wave-I amplitude to capture all aspects of CS, as noise-induced CS might
114 preferentially affect LSR AN fibers (Furman et al., 2013).

115 This study proposes the use of a relative derived-band EFR method
116 (DBEFR), to confine the EFR to a specific frequency band. We hypothesize
117 that the relative metric design of the DBEFR reduces the impact of subject-
118 specific factors and increase its sensitivity to individual sensorineural hearing
119 deficits. DBEFR magnitudes were extracted from individuals in four groups
120 to study their applicability to diagnose sensorineural hearing deficits: (1) a
121 young normal-hearing control group, (2) a group with self-reported hearing

122 difficulties in noisy environments, (3) a group of older listeners with nor-
123 mal audiograms and (4) an age-matched group with sloping high-frequency
124 audiograms. We assumed that the second group might be affected by CS
125 due to noise overexposure or ageing and that the third group might be af-
126 fected by age-induced CS, without co-occurring OHC damage. Aside from
127 collecting DBEFRs, we assessed individual OHC function using audiomet-
128 ric and DPOAE thresholds. In line with animal studies of age-related and
129 noise-induced synaptopathy, we expect that the DBEFR will be reduced in
130 all but the control group. However, a direct assessment of the individual de-
131 gree of OHC and AN damage is impossible and hence we complemented our
132 experimental work with a modelling approach to better understand the re-
133 lationship between sensorineural pathologies and their effect on the DBEFR
134 magnitudes. Models can study the impact of AN fibers and sensory hair cells
135 damage on the EFR generators independently and concomitantly to under-
136 stand their respective roles on DBEFR generation (Verhulst et al., 2016,
137 2018a,b). We adopt a biophysically inspired model of the human hearing
138 periphery calibrated for ABR and EFR simulation (Verhulst et al., 2018a)
139 and considered the simulations together with the data to interpret the im-
140 plications of our findings for DBEFR-based hearing diagnostics.

141 **2. Materials and Methods**

142 Two experiments were conducted at two recording locations. In the first
143 experiment (University of Ghent), normal-hearing (NH) and listeners with
144 self-reported hearing difficulties (NHSR) participated. In the second experi-
145 ment (University of Oldenburg), a total of 43 participants were recruited in

146 three groups: a young NH control group (yNH), an older NH group (oNH)
147 and an older group with sloping high-frequency audiogram (oHI). Ethical ap-
148 provals were obtained from University of Ghent and Oldenburg and all par-
149 ticipants were informed about the experimental procedure and an informed
150 consent was obtained from each subject before the experiment.

151 *2.1. Participants*

152 16 NH listeners with ages between 18 and 30 (NH: 24.21 ± 4.10 years, five
153 females) and 9 NH subjects with self-reported hearing difficulties (NHSR)
154 with ages between 23 to 49 (NHSR: 33.78 ± 8.57 years, three females) par-
155 ticipated in the first experiment. The NHSR participants were recruited
156 using a flyer asking whether they had speech understanding difficulties in
157 the presence of background noise, while not presently being treated for hear-
158 ing disorders. Measurements were conducted in two sessions per subject,
159 with a maximum sound exposure time of 90 minutes per session. The partic-
160 ipants filled out a questionnaire, in which they were asked how often (yearly,
161 monthly, weekly or daily) they had been playing a musical instrument in
162 a band, attended festivals, concerts or discotheques and used noisy tools
163 during their lifetime. Moreover, the total number of noise-exposed sessions,
164 their duration and estimated noise loudness (a score between 1 to 5) were also
165 obtained (Degeest et al., 2014). Audiograms were measured with an Inter-
166 acoustics Clinical Computer Audiometer (AC5) at ten standard frequencies
167 between 0.25 and 8 kHz.

168 The second experiment was conducted with three participant groups com-
169 posed of: 15 young normal-hearing (yNH: 24.53 ± 2.26 years, eight female),
170 16 old normal-hearing (oNH: 64.25 ± 1.88 years, 8 female) and 12 old hearing-

171 impaired (oHI: 65.33 ± 1.87 years, seven female) participants. All yNH partic-
172 ipants had pure-tone thresholds below 20 dB-HL at all measured frequencies
173 between 0.125 and 10 kHz (Auritec AT900, Hamburg, Germany audiome-
174 ter). In both experiments, the audiometrically better ear was chosen for the
175 experiment and stimuli were presented monaurally while participants were
176 seated in a comfortable chair in an acoustically and electrically shielded sound
177 booth, watching silent movies with subtitles to stay awake. Figure 1 shows
178 audiograms of the subjects in all groups. From here on, \triangle stands for the NH
179 group in the first experiment, \square for NHR group, \diamond for yNH in the second
180 experiment, \circ for oNH and \triangleleft for oHI group.

181 2.2. Distortion Product Otoacoustic Emissions (DPOAEs)

182 In the first experiment, DPOAEs were recorded to ten primary-level pairs,
183 (L_1 , L_2), at nine primary-frequency pairs: $f_2 = [546, 780, 1002, 1476, 1998,$
184 $3012, 3996, 6006, 8003]$ and $f_1 = f_2/1.2$. L_2 ranged from 20 to 65 dB-SPL
185 in 5 dB steps and $L_1 = 0.4L_2 + 39$ dB, according to the scissors paradigm
186 (Kummer et al., 1998). The nine primary frequency pairs were chosen to
187 have complete stimulus periods of the primaries in each pair. For each fre-
188 quency and level pair, 45 repetitions were generated in MATLAB 2016b and
189 an ER-10X extended-bandwidth Etymotic Research probe system was used
190 to deliver the two pure tones via a loudspeaker/microphone probe inserted
191 in the ear-canal using a silicone eartip. The response was recorded and dig-
192 itized using a Fireface UCX external sound card (RME). The pure tones
193 were calibrated separately using a B&K artificial ear and B&K sound level
194 meter at each primary frequency, separately. The time-domain ear-canal
195 recordings were converted to pressure using the microphone sensitivity (50

196 $\frac{\text{mV}}{\text{Pa}}$) and pre-amplifier gain (40 dB). Then, I/O functions were calculated for
197 the measured primary-frequency pairs by defining the L_{DP} as the averaged
198 spectrum magnitude at the $2f_1$ - f_2 cubic distortion frequency, multiplied by
199 $\frac{2}{N\sqrt{2}}$, where N is the number of samples at each f_2 response. Finally, a lin-
200 ear function $L_{\text{DP}}=aL_2+b$ was fit to the bootstrapped data-points and the
201 crossing point with $L_{\text{DP}}=0$ Pa was defined as the DPOAE threshold at the
202 measured f_2 frequency. DPOAEs in the second experiment were acquired
203 using a custom-made software (Mauermann, 2013) which implements a pri-
204 mary frequency sweep method at a fixed f_2/f_1 of 1.2 (Long et al., 2008).
205 The primary frequencies were swept across an 1/3 octave range around the
206 $f_2 = 4\text{kHz}$ geometric mean with a duration of 2s/octave Primary levels were
207 chosen according to the scissors paradigm (Kummer et al., 1998). DPOAE
208 thresholds were calculated by fitting a linear function to the bootstrapped
209 data-points and was extrapolated to cross $L_{\text{DP}}=0$ Pa. Additional details on
210 the experimental procedure can be found in Verhulst et al. (2016).

211 *2.3. Envelope Following Responses (EFRs)*

212 The EFR stimuli in the first experiment were five filtered 70 dB-SPL
213 white noise carriers, which were 100% modulated with a 120-Hz sinusoid. To
214 generate them, the white noise was filtered between the following frequency
215 regions: [0.25-22], [0.5-22], [1-22], [2-22] and [4-22] kHz, using a 1024th order
216 FIR band-pass filter designed by the Blackman-window method. In each fre-
217 quency band, a stimulus with a duration of 1.25 s was generated in MATLAB
218 2016b, windowed with a 1.25% cosine-tapered window and delivered monau-
219 rally over ER-2 earphones, connected to a Fireface UCX external sound card
220 (RME) and a TDT-HB7 headphone driver. A uniformly-distributed random

221 silence jitter was applied between consecutive epochs ($200\text{ ms}\pm 20\text{ ms}$) of the
222 370 stimulus presentations. The stimuli were calibrated to have the same
223 spectral magnitude using a B&K sound-level-meter type 2606. Hence, the
224 narrower stimuli had lower sound pressure levels than the broader condition.
225 Figure 2a shows spectral illustration of the designed stimuli. Scalp-recorded
226 potentials were obtained with a 64-Channel Biosemi EEG recording system
227 and a custom-built trigger box using a sampling frequency of 16384 Hz. The
228 electrodes were placed according to the 10-20 standard, using highly conduc-
229 tive gel (Signa gel). The Common Mode Sense (CMD) and Driven Right
230 Leg (DRL) electrodes were placed on top of the head. Six external channels
231 were used as well, i.e. two earlobe electrodes as reference and the remaining
232 electrodes were placed on the forehead and cheeks to record electrical ac-
233 tivity induced by horizontal and vertical eye movements. All channels were
234 re-referenced to the average of the two earlobe electrodes.

235 In the second experiment, four EFR stimuli with white noise carriers were
236 band-pass filtered using the same filter as in the first experiment in $[\frac{0.5}{\sqrt{2}},$
237 $16]$, $[\frac{1}{\sqrt{2}}, 16]$, $[\frac{2}{\sqrt{2}}, 16]$ and $[\frac{4}{\sqrt{2}}, 16]$ kHz frequency regions. Stimuli were
238 95% modulated with a 120-Hz pure tone and presented at 70 dB SPL using
239 the same configuration as the first experiment. The stimuli had a duration
240 of 400 ms, were 2.5% ramped with a tapered-cosine window and presented
241 1000 times using a uniformly distributed random inter-stimulus silence jit-
242 ter of $100\text{ ms}\pm 10\text{ ms}$. The calibration was performed in the same way as
243 for the first experiment, but using B&K sound level meter type 2610. A
244 64-channel Biosemi EEG system was adopted to record the responses using
245 EEG caps with equidistant electrode spacing. The CMS and DRL electrodes

246 were located on the fronto-central midline and on the tip of the nose of the
247 participants, respectively.

248 **3. EFR Analysis**

249 Acquired EFRs were first filtered using an 800th order Blackman window-
250 based FIR filter between 60 and 600 Hz, using the *filtfilt* function of MAT-
251 LAB to avoid time delays and phase shifts. Signals were broken into 1-s
252 long epochs relative to the trigger onset, from 0.25 to 1.25 s in the first and
253 into 0.3-s long epochs, from 0.1 to 0.4 s in the second experiment. Baseline
254 correction was applied before the epochs were averaged across trials. 30 and
255 100 epochs were rejected on the basis of the highest peak-to-trough values
256 in the first and second experiment, respectively. Since the firing patterns of
257 neurons are influenced by factors such as instantaneous external inputs, pre-
258 vious firing patterns and the general state of the system, the interpretation
259 of the raw EFR spectrum resulting from the Fast Fourier Transform (FFT)
260 of the averaged epochs is challenging. Synaptic delays and axon conduction
261 limitations cause a $\frac{1}{f}$ behaviour in EEG (Buzsaki, 2006, Chapter 10) and it is
262 crucial to suppress this noise-floor to analyse the stimulus-driven spectrum.
263 The bootstrapping approach proposed in Zhu et al. (2013) was employed to
264 estimate the $\frac{1}{f}$ noise-floor component. First, 340 epochs were drawn ran-
265 domly with replacement, among the 340 epochs (900 epochs in the second
266 experiment). Then, the FFT of these epochs were averaged. This procedure
267 was repeated $N_1=200$ times ($N_2=400$ for the second experiment), resulting in
268 a nearly Gaussian distribution of raw, averaged spectra. The average value
269 of this distribution yielded the frequency domain representation of the EFRs.

270 Afterwards, the same procedure with $M_1=1000$ repetitions ($M_2=1200$ for the
271 second experiment) and phase-flipped (180°) odd epochs was followed to esti-
272 mate the spectral noise-floor as a function of frequency. The idea behind this
273 approach is that the time-locked response is suppressed if the averaging is
274 repeated sufficiently across phase-inverted epochs. Finally, the averaged ab-
275 solute values of the estimated noise floors were subtracted from the averaged
276 absolute values of the EFR spectra amplitudes to obtain the stimulus-driven
277 EFR spectrum:

$$\text{EFR}_{\text{Spec}}(f) = \frac{2}{n_p} \left(\left| \frac{\sum_{i=1}^N \text{FFT}(X_i)}{N_p} \right| - \left| \frac{\sum_{j=1}^M \text{FFT}([-1]^j X_j)}{M_p} \right| \right) \quad (1)$$

278

279 X represents the epochs vector, N the number of bootstrap repetitions, M the
280 number of repetitions to estimate the noise-floor, p the experiment number
281 (i.e. one or two) and n equals the number of FFT points ($n_1=16384$ and
282 $n_2=8192$).

283 EFR_{Spec} peak values, which were four standard deviations above the noise-
284 floor at 120 Hz, i.e. the modulation frequency, and the following two har-
285 monics at 240 and 360 Hz, were added to yield EFR magnitude of the cor-
286 responding condition.

$$\text{EFR}_{\text{PtN}} = \sum_{k=0}^2 \text{EFR}_{\text{Spec}}(f_k), \quad f_k = 120 \times (k + 1) \quad (2)$$

287 To construct DBEFRs, the calculated EFR_{PtN} for each narrower-band
288 condition was subtracted from the following wider-band condition using:

$$\text{DBEFR}_{\text{PtN}} = \begin{cases} (\text{EFR}_{\text{PtN}})_{\text{wide}} - (\text{EFR}_{\text{PtN}})_{\text{narrow}}, & (\text{EFR}_{\text{PtN}})_{\text{wide}} > (\text{EFR}_{\text{PtN}})_{\text{narrow}} \\ 0, & (\text{EFR}_{\text{PtN}})_{\text{wide}} \leq (\text{EFR}_{\text{PtN}})_{\text{narrow}} \end{cases} \quad (3)$$

289 Derived frequency bands from EFRs to the first experimental stimuli are
290 shown schematically in Fig. 2b.

291 **4. Questionnaire analysis**

292 The completed questionnaires from the participants in the first experi-
293 ment were used to estimate the individual life-time noise exposure dose. To
294 this end, the collected individual data related to the frequency and duration
295 of experienced noise exposure were converted to a number of sessions per year
296 multiplied by the duration and the personal estimated noise loudness scores,
297 i.e. a number between 1 and 5. We followed the procedures as described in
298 Degeest et al. (2014). The scores were separately calculated for questionnaire
299 categories: (i) playing musical instrument in a band, (ii) attending festivals,
300 concerts and discotheques and (iii) using noisy tools. Outcomes were nor-
301 malized across NH and NHR groups participants by the highest reported
302 dose, i.e. 30600, 18480 and 26000 hours in each category, respectively.

303 **5. Model Simulations**

304 A biophysical model of the human auditory periphery (Verhulst et al.,
305 2018a), schematically shown in Fig. 3, was adopted to simulate the experi-
306 mental conditions and to investigate the effect of different aspects of sen-
307 sorineural hearing deficits on the EFR_{PtN} and $\text{DBEFR}_{\text{PtN}}$ magnitudes. The

308 original implementation of the model is described in Verhulst et al. (2018a)
309 and can be downloaded from “[https://github.com/HearingTechnology/Ver-](https://github.com/HearingTechnology/Verhulstetal2018Model)
310 *hulstetal2018Model*”. The parameters which determine the weights between
311 the population AN, cochlear nucleus (CN) and inferior colliculus (IC) re-
312 sponses were adjusted along with the AN innervation patterns across CF for
313 the purpose of this study.

314 5.1. Auditory nerve-fiber distribution

315 The original model implementation introduced the same number of synapses
316 between inner-hair-cells (IHCs) and AN fibers for all simulated characteristic
317 frequencies (CF), whereas human and rhesus monkey innervation patterns
318 show a bell-shaped pattern across CF. To make the model more realistic,
319 the averaged synaptic counts of four control rhesus monkeys (seven ears)
320 and nine frequencies (Valero et al., 2017) were mapped to corresponding
321 fractional distances of the human cochlea using the monkey place-frequency
322 map (Greenwood, 1990). Fractional distances from the base of cochlea, d_i ,
323 were calculated according to the measured frequency points (f_{RM_i}):

$$f_{RM_i}[\text{in Hz}] = 360(10^{2.1(1-d_i)} - 0.85), \quad i = 1, 2, \dots, 9 \quad (4)$$

324

325 The obtained d_i s were substituted into the analogous Greenwood map equa-
326 tion for humans, yielding the corresponding frequency points (f_{H_i}):

$$f_{H_i}[\text{in Hz}] = 165.4(10^{2.1(1-d_i)} - 0.88), \quad i = 1, 2, \dots, 9 \quad (5)$$

327 To calibrate the model with the applied AN pattern, a 70 dB-nHL click-
328 train containing both stimulus polarities was presented at a rate of 11 Hz.
329 To perform this calibration, simulated ABR wave amplitudes were matched
330 to the experimental data on the basis of 55 averages. Specifically, the
331 $M_1 = 4.6729 \times 10^{-14}$, $M_3 = 5.6885 \times 10^{-14}$ and $M_5 = 14.641 \times 10^{-14}$ param-
332 eters were adjusted on the basis of average NH ABR wave-I, III and V
333 reference data from Picton (2010), i.e. $w_I = 0.15\mu V_p$, $w_{III} = 0.17\mu V_p$ and
334 $w_V = 0.61\mu V_{pp}$.

335 Using the synapse counts from rhesus monkey and the mapped frequency
336 points for the human cochlea (f_{Hi}), a “smoothing spline” curve was fit to esti-
337 mate the number of synapses across all frequency channels in the model. Fi-
338 nally, to simulate different AN fiber types, i.e. high spontaneous-rate (HSR),
339 medium spontaneous-rate (MSR) and LSR fibers, and their properties, the
340 obtained population distribution was multiplied by the corresponding AN
341 type proportion factor C , i.e. $C_{HSR} = 0.60$, $C_{MSR} = 0.25$ and $C_{LSR} = 0.15$
342 (Lieberman, 1978, cat data), before responses were summed at each simu-
343 lated CF and fed to the CN model. The simulated frequency-specific AN
344 fibers distribution is shown on the top-right column of Fig. 3.

345 5.2. Stimuli

346 The model stimuli were matched to the experimental conditions and had
347 a duration of 600-ms in the first experiment (95% modulated and 400-ms
348 for the second experiment). Twenty stimulus repetitions with different white
349 noise iterations were applied to the model and simulations were averaged
350 before the EFR_{PtN} was calculated using the same procedure as in Eq. 2. The
351 amplitudes of the model stimuli were set based on the broadest condition, i.e.

352 0.25 to 22 kHz for the first experiment and 0.353 to 16 kHz for the second
353 experiment to yield an input of 70 dB SPL. The narrower band stimuli were
354 calibrated relative to the broadest condition, such that they had the same
355 spectral level as the broadband condition but with a different SPL.

356 *5.3. Simulating sensorineural hearing loss*

357 The simulated CS profiles and their corresponding AN fiber types are
358 shown in Fig. 3. Different degrees of CS were modelled by manipulating the
359 number and types of the AN fibers. The table in Fig. 3 shows the simu-
360 lated synaptopathy profiles. OHC damage was simulated by changing the
361 CF-dependent mechanical gain of the cochlea by moving poles of the BM
362 admittance function to yield a filter gain reduction corresponding to a de-
363 sired dB-HL-loss, which also yielded wider cochlear filter. The inset in Fig. 3
364 shows the simulated cochlear gain loss profiles. Procedures are detailed in
365 (Verhulst et al., 2016, 2018a).

366

367 **6. Results**

368 *6.1. EFR and dependence on stimulus frequency*

369 Figure 4 shows individual and group-mean EFR_{PtN} magnitudes to dif-
370 ferent frequency bandwidths in the first (panel a) and second (panel b) ex-
371 periments. Despite within-group individual variability, experimental group-
372 means revealed approximately constant EFR_{PtN} magnitudes to stimuli with
373 frequencies below 2 kHz and reduced magnitudes to frequencies above 2 kHz
374 and 2.828 kHz in the first and second experiment, respectively. A paired-
375 sample t-test with Bonferroni correction was applied to compare EFR_{PtN}

376 magnitudes to stimuli with different frequency bandwidths in each group.
377 In the first experiment, a single significant difference was observed between
378 the $EFR_{[2-22]}$ and $EFR_{[4-22]}$ conditions in NH group ($t(11)=7.02$, $p<0.0000$),
379 which disappeared for the NHR group ($t(8)=3.13$, $p=0.014$). In the second
380 experiment, a paired-sample t-test with Bonferroni correction gave a signif-
381 icant difference between $EFR_{[2.828-16]}$ and $EFR_{[5.656-16]}$ in yNH ($t(12)=7.86$,
382 $p<0.0000$) and oNH groups ($t(12)=6.21$, $p<0.0000$), but not in the oHI group
383 ($t(9)=2.03$, $p=0.07$). Simulated NH-EFRs are shown in hexagons in Fig. 4
384 and corroborate experimental findings by showing a minor contribution of
385 stimulus frequencies below 2 kHz on the EFR generation .

386 6.2. Derived-Band Envelope Following Responses (DBEFRs)

387 $DBEFR_{PtN}$ magnitudes calculated using Eq. 3 are shown in Fig. 5 for
388 the first and second experiment. A paired-sample t-test with Bonferroni
389 correction comparing the EFR_{PtN} magnitudes in each group revealed only
390 a significant difference between the [1-2] and [2-4] kHz condition in the NH
391 group ($t(12)= -3.99$, $p=0.002$). In the second experiment, paired-sample
392 t-test showed significant difference between [0.353-0.707] and [2.828-5.656]-
393 kHz conditions only in yNH group ($t(11)=-7.00$, $p<0.000$). In support of
394 our experimental findings, simulated NH-DBEFR magnitudes in both ex-
395 periments (shown by hexagons Fig. 5a and b) were equal for derived-bands
396 below 2-kHz and increased for $DBEFR_{[2-4]}$ (in the first experiment) and
397 $DBEFR_{[2.828-5.656]}$ (in the second experiment). In line with EFR_{PtN} find-
398 ings in Section 6.1, experimental and simulated $DBEFR_{PtN}$ magnitudes in
399 both experiments showed an increased contribution of the [2-6] kHz derived
400 frequency band to the EFR generation.

401 *6.3. Possible origins of individual EFR differences*

402 Previous studies have shown a dependency of the scalp-recorded AEP
403 magnitude to head size, sex and age (Trune et al., 1988; Mitchell et al., 1989;
404 Makary et al., 2011) and possible coexisting aspects of CS and OHC dam-
405 age (Parthasarathy and Kujawa, 2018; Vasilkov and Verhulst, 2019). Hence,
406 the spread of data-points within different recorded test-groups and spectral
407 bandwidths could be explained by subject-specific factors unrelated to hear-
408 ing or hearing-related factors associated with the main factors for grouping:
409 (i) self-reported hearing difficulties in noisy environments in the first experi-
410 ment, (ii) age and (iii) elevated hearing thresholds in the second experiment.
411 Pooling together the NH and NHR EFR_{PtN} magnitudes, a regression anal-
412 ysis was conducted to investigate the effect of age, 4 kHz threshold, head
413 size and DPTH₃₀₀₀ on the EFR_[2-22] (Fig. 6, left column) and DBEFR_[2-4]
414 magnitude (Fig. 7, left column). None of the regressions showed a relation
415 between tested variables, suggesting that other factors than those reported
416 were responsible for the individual variability among listeners. The regression
417 analysis on EFR_{PtN} and DBEFR_{PtN} magnitudes combined from all experi-
418 mental groups in the second experiment (Fig. 6 and 7, right column) showed
419 a meaningful correlation of age, threshold, head size and DPTH₄₀₀₀ with the
420 EFR_[2.828-16] magnitude. However, extracting the DBEFR_[2.828-5.656], reduced
421 the correlation with age or 4-kHz threshold and suppressed any meaningful
422 correlation with head-size and DPTH₄₀₀₀. Moreover, excluding the oHI group
423 from the correlation analysis, led to a reduced and insignificant correlation co-
424 efficient (R=-0.38, p=0.083) between 4-kHz threshold and DBEFR_[2.828-5.656].
425 These results suggest that the proposed DBEFR metric is not affected by

426 head size. Individual variabilities between the yNH and oNH groups in the
427 second experiment might be related to degraded temporal envelope coding
428 as a consequence of CS (Bharadwaj et al., 2015), given the insignificant cor-
429 relations of DBEFRs with the 4-kHz threshold, $DPTH_{4000}$ and head size.

430 *6.4. EFR_{PtN} and $DBEFR_{PtN}$ magnitude variability across tested groups*

431 To investigate the separability of the recruited groups by means of their
432 DBEFR magnitudes, we analysed the group-mean differences in each exper-
433 iment. In the first experiment, an independent two-sample t-test compari-
434 son between the means of stimulated frequency bandwidths in the NH and
435 NHSR group (Fig. 4a), showed a significant difference only between the [2-22]
436 and [4-22]-kHz conditions ($EFR_{[2-22]}$: $t(19)=3.36$, $p=0.003$ and $EFR_{[4-22]}$:
437 $t(19)=2.76$, $p=0.012$). However, significant mean-differences disappeared
438 between similar conditions in the NH and NHSR groups after extracting
439 DBEFR magnitudes in Fig. 5a ($DBEFR_{[2-4]}$: $t(19)=-0.90$, $p=0.338$). The
440 insignificant difference across groups and insignificant correlation coefficients
441 of $DBEFR_{[2-4]}$ with subject-specific factors observed in Fig. 7, might partly
442 be explained by the different amounts of experienced lifetime noise expo-
443 sure reported in the questionnaires and might point to various degrees of
444 noise-induced CS. Although calculated noise scores in Fig. 8 revealed an in-
445 significant correlation with $DBEFR_{[2-4]}$ magnitudes ($R=0.13$, $p=0.089$), the
446 highest levels of noise dose were associated with degraded $DBEFR_{[2-4]}$ mag-
447 nitudes and increased standard errors in NH (e.g. subject No. 12) and NHSR
448 group (e.g. subjects No. 7 and 9), even though no complaints of hearing diffi-
449 culties in noisy environments were reported by the NH listeners. In addition,
450 the elevated DBEFR magnitudes observed in the NHSR group, were obtained

451 for people with low noise scores (e.g. subject No. 1 in NHSR group), de-
452 spite their reports of hearing difficulties in noisy environments. Therefore, we
453 ascribe the overlapping DBEFR magnitudes in NH and NHSR groups, and
454 consequent insignificant group-means to the insufficient number of the sam-
455 ples and a subject-dependent unreliable discriminating factor between the
456 two groups, i.e. subjective reporting of hearing complaints in noisy environ-
457 ments (Coughlin, 1990) and variability in answering lifetime noise-exposure
458 dose questionnaires (Prendergast et al., 2017; Bramhall et al., 2017).

459 In the second experiment, an independent two-sample t-test was applied to
460 investigate the effect of age between the yNH and oNH groups, and elevated
461 high-frequency thresholds between the oNH and oHI groups. This compar-
462 ison showed a significant effect of age in all frequency bandwidths and a
463 significant effect of hearing threshold in all frequency bands except for the
464 [2.828-16] kHz band ($t(21) = -1.81$, $p = 0.08$). The same comparison for the
465 DBEFR magnitudes revealed a significant effect of age and hearing threshold
466 only in the [2.828-5.656]-kHz derived band condition ($t(23) = 3.13$, $p=0.004$
467 and $t(21) = -4.60$, $p = 0.002$, respectively), consistent with the correlation
468 presented in Fig. 7.

469 Our group-mean results combined with the correlation analysis in Section 6.3
470 suggests that the DBEFR metric removes inter-subject variability unrelated
471 to hearing between yNH and oNH groups, but leaves individual magnitude
472 differences within a group meaningful, given the often non-overlapping stan-
473 dard deviations. Consequently, the significant group-mean difference between
474 yNH and oNH might reflect individual degrees of sensorineural hearing loss.
475 To investigate the diagnostic sensitivity, it is of course necessary to under-

476 stand the respective role of OHC deficits and CS on DBEFR magnitudes.
477 Given that oHI listeners may suffer from both OHC deficits and CS, it is
478 important to study the impact of OHC-damage and CS both independently
479 and concomitantly.

480 *6.5. The EFR relationship to different aspects of sensory hearing-loss*

481 Since OHC-damage and CS might both affect the EFR magnitude (Gar-
482 rett and Verhulst, 2019; Vasilkov and Verhulst, 2019), we employed a com-
483 putational model of the auditory periphery to simulate how different degrees
484 of CS affected the EFR_{PtN} magnitude, both in presence and absence of high-
485 frequency sloping OHC-loss above 1 kHz (simulated high-frequency slop-
486 ing audiograms in Fig. 3). Only EFRs generated from the most frequency-
487 sensitive regions of the cochlea, namely the [2-22] and [4-22] kHz conditions
488 in the first experiment (Fig. 9a) and [2.828-16] and [5.656-16] kHz in the sec-
489 ond experiment (Fig. 9b) were considered. Model simulations showed that
490 CS, when no other hearing deficits co-occur, reduces the EFR and DBEFR
491 magnitudes. Applying sloping high-frequency OHC-damage increased the
492 DBEFR magnitudes in both experiments (Fig. 9c and d). According to the
493 simulations, the NH DBEFR magnitude reduced by 46% as a consequence of
494 losing 47% of the AN fibers (i.e., the 10-0-0 CS profile defined in Fig. 3), while
495 the Slope20 OHC-damage (defined in Fig. 3) increased the NH DBEFR mag-
496 nitude by 27%. Hence, the effect of OHC-damage on the DBEFR magnitude
497 is smaller than CS alone, however it is not negligible. Therefore, the exper-
498 imental range of individual EFR and DBEFR magnitudes can be explained
499 by the different degrees of variation simulated by CS and OHC-damage.
500 Simulations captured both the experimental absolute magnitudes and DBE-

501 FRs and explained the experimental differences between yNH and oNH groups
502 on the basis of age-induced CS and not OHC-damage differences. Further,
503 the simulations suggest that oNH and oHI listeners might both suffer from
504 CS. Results are less clear for the NHSR group where there is a strong over-
505 lap with the NH group. However the noise scores from the questionnaires
506 in Fig. 8, could ascribe some spread of DBEFR magnitudes in the NH and
507 NHSR groups to noise-induced CS and to a lesser degree to OHC-damage,
508 given that they all had normal hearing thresholds.

509 It is worthwhile to note that EFR magnitudes in both experiments (Fig. 3a
510 and c), decreased as a result of CS alone and increased by applying high-
511 frequency OHC-damage with a severity of less than 20 dB-HL at 8 kHz.
512 However, higher degrees of OHC-damage reduced the EFR magnitudes. We
513 explain this non-monotonic behaviour on the basis of the AN fiber discharge
514 rate-level curve, where increased simulated EFR_{PtN} magnitudes (Fig. 9 c and
515 d) and amplitude-modulated (AM) responses (Fig. 10b) to supra-threshold
516 stimuli (70 dB-SPL) caused by OHC-damage, might stem from the extended
517 dynamic range of the AN fibers for less effective AN-driving levels (Bharad-
518 waj et al., 2014, their Fig.3c). Given that experimental and simulated stimuli
519 were calibrated to have equal spectral magnitudes for all stimulus band-
520 widths, the narrowest stimulus was presented at a lower overall sound level
521 than the 70 dB-SPL broadband stimulus. Applying more severe OHC-loss,
522 shifted the AN discharge rate and envelope synchrony strength to the enve-
523 lope to lower values (Verhulst et al., 2018a, Fig.5) and decreased the EFR
524 magnitudes (Verhulst et al., 2018a, their Fig.7). However, DBEFR mag-
525 nitudes increased monotonically for all simulated degrees of OHC damage

526 (Fig. 9c and d).

527 **7. Discussion**

528 *7.1. Tonotopic sensitivity of the EFR generators*

529 Despite the individual variability within groups, experimental group-
530 mean EFR_{PtN} magnitudes to broadband stimuli with different bandwidths
531 (Fig. 4a), were equal at frequencies below 4 kHz and reduced in response to
532 [4-22] kHz condition. In the second experiment (Fig. 4b), the EFRs remained
533 equal at frequencies below 5.656 kHz and degraded when the [5.656-16] kHz
534 band was added. Consequently, equal $DBEFR_{PtN}$ magnitudes were obtained
535 for frequencies below 2 kHz. Individual variability was best observed for
536 the $DBEFR_{PtN}$ extracted from the [2-4] kHz (first experiment, Fig. 5a) and
537 [2.828-5.656] kHz (second experiment, Fig. 5b) frequency bands. Simulated
538 EFRs to the experimental stimuli shown with hexagons in Fig. 4 and 5, con-
539 firmed observed experimental EFR_{PtN} and $DBEFR_{PtN}$ frequency-dependent
540 behaviour. In addition, the model can be used to study which CF regions
541 along the cochlea contributed strongly to the population EFR response. To
542 this end, we calculated the AM (Fig. 5a) and derived-band AM (DBAM)
543 responses at each CF (Fig. 5b) as follows:

$$AM_{AN}(N_{CF}) = \frac{1}{n} \sum_{i=0}^2 [2|\text{FFT}(AN_{N_{CF}})|]_{f_i}, \quad (6)$$

$$N_{CF} = 1, 2, \dots, 401, f_i = 120 \times (i + 1)$$

$$DBAM_{AN} = |MR_{AN}(\text{wide}) - MR_{AN}(\text{narrow})| \quad (7)$$

544 $AN_{N_{CF}}$ is the AN-response at N_{CF} channel and $n = n_1$ as was defined in
545 Eq. 1. These simulations corroborate the experimentally-observed minor
546 contribution of low-frequency CF channels to the EFR generation.

547 In a previous modelling study, we investigated the tonotopic sensitivity
548 of EFR_{P_tN} to broadband stimuli and ascribed the poor low-frequency AM
549 coding to a combination of the chosen modulation frequency (120 Hz) and
550 the narrower bandwidth of apical cochlear filters compared to the higher CF
551 filters (Moore and Glasberg, 1983). Model simulations in response to the
552 spectrally broadest condition, i.e. [0.25-22] kHz, modulated with a range
553 of lower modulation frequencies than 120-Hz, suggested that despite an en-
554 hanced modulated response at BM, the saturation properties of AN fibers
555 limited the modulation response at all modulation frequencies at higher CFs.
556 This resulted in a degraded response at carrier frequencies above 4 kHz and
557 shifted the frequency sensitivity to the lower CFs at low modulation frequen-
558 cies (Keshishzadeh et al., 2019). Since the brain response to modulation fre-
559 quencies below 70 Hz may contain cortical as well as brainstem contribution
560 (Purcell et al., 2004; Picton, 2010, Chapter 10), employing low modulation
561 frequencies might render EFR-based CS diagnosis insensitive, even though
562 an improved frequency-sensitivity can be obtained from the apical regions
563 using these lower modulation frequencies. Therefore, the employed experi-
564 mental modulation frequency, i.e. 120-Hz in combination with a broadband
565 carrier, might be able to establish a frequency-specific CS diagnosis at fre-
566 quencies above 2 kHz (Keshishzadeh et al., 2019). In this context, the pro-
567 posed DBEFR method showed a notable contribution of the [2-4] kHz CF
568 region ([2.828-5.656] kHz in the second experiment) to the EFRs generation

569 by showing a significantly stronger DBEFR_{PtN} magnitude compared to lower
570 derived-band conditions in the NH group.

571 *7.2. Diagnostic Application*

572 The measured DBEFR magnitudes are individually separable and above
573 the noise-floor even for HI listeners, whose group-mean was significantly
574 above the noise-floor (Section 6.4). In addition, the DBEFR offers a frequency-
575 specific metric in the [2-6] kHz region to assess supra-threshold temporal
576 coding of the population of AN fibers and brainstem neurons. Despite these
577 promising results, the diagnostic sensitivity of DBEFRs also has limitations.
578 The proposed DBEFR magnitude is sensitive to CS alone, when no other
579 coexisting hearing deficits occur and is hence applicable for use in ageing
580 listeners with normal audiograms and those with self-reported hearing dif-
581 ficulties or prone to noise exposure. However, DBEFRs are also affected
582 by OHC damage. The metric hence needs to be complemented with another
583 supra-threshold metric sensitive to OHC damage to allow a separation of both
584 the CS and OHC aspect of sensorineural hearing deficit from the DBEFR
585 recorded from listeners with impaired audiograms (e.g. Vasilkov and Ver-
586 hulst, 2019).

587 Lastly, the employed high modulation frequency, i.e. 120 Hz, suppresses cor-
588 tical contributions to the EFR_{PtN} magnitudes, but also degrades AM-coding
589 from lower CFs and thereby limits tonotopic sensitivity of the EFR_{PtN} to
590 frequencies above 2 kHz. Consequently, apical-end supra-threshold hear-
591 ing deficits would not be reflected in the proposed DBEFR_{PtN} metric even
592 for stimuli which contain frequencies below 2 kHz. These results are con-
593 sistent with the source generators of derived-band ABRs (DBABR), which

594 degrades in amplitude for bands below 2 kHz (Don and Eggermont, 1978).
595 This predominant basal origin of the ABR also confines the potential of
596 ABR/DBABR-based CS diagnosis (i.e. wave-I amplitude) to basal cochlear
597 regions.

598 **8. Conclusion**

599 We proposed the use of a relative DBEFR_{PtN} metric to render the EFR_{PtN}
600 frequency-specific and rule out subject-specific factors unrelated to hearing to
601 apply it in the study of the origins of sensorineural hearing deficits and their
602 role in supra-threshold temporal envelope encoding. DBEFR_{PtN} magnitudes
603 from two experiments were analysed and compared to model simulations to
604 conclude that the frequency-sensitivity of DBEFR_{PtN} magnitudes to broad-
605 band stimuli is limited to the [2-6] kHz bandwidth. Secondly, we showed
606 that the DBEFR metric eliminates inter-subject variability due to hearing
607 unrelated sources. Model simulations (Fig. 3) explained the significant dif-
608 ference between yNH and oNH listeners on the basis of CS, which could
609 relate to age-induced CS in line with human post-mortem studies (Makary
610 et al., 2011; Viana et al., 2015; Wu et al., 2019). Supported by model predic-
611 tions (Fig. 9d), the significant differences between age-matched oNH and oHI
612 groups was explained by OHC-damage and coexisting CS as a consequence of
613 ageing. Accordingly, profound OHC damages may confound DBEFR-based
614 clinical applications of CS diagnosis. Despite this limitation in the differen-
615 tial diagnosis of CS and OHC deficits on the basis of the DBEFR magnitude,
616 the proposed metric can be used to diagnose CS in a frequency-specific man-
617 ner in listeners with thresholds below 20 dB-HL. Moreover, it provides an

618 objective marker of supra-threshold temporal envelope coding ability, which
619 can be used to study its role in sound perception studies. Lastly, our results
620 clearly demonstrate that older listeners with or without impaired audiograms
621 suffer from degraded temporal envelope coding at frequencies above 2 kHz.

622 **Acknowledgement**

623 Work supported by European Research Council starting grant ERC-StG-
624 678120 (RobSpear).

625 **References**

- 626 Abdala, C. and Folsom, R. C. (1995). The development of frequency resolu-
627 tion in humans as revealed by the auditory brain-stem response recorded
628 with notched-noise masking. *The Journal of the Acoustical Society of*
629 *America*, 98(2):921–930.
- 630 Bharadwaj, H. M., Masud, S., Mehraei, G., Verhulst, S., and Shinn-
631 Cunningham, B. G. (2015). Individual differences reveal correlates of hid-
632 den hearing deficits. *Journal of Neuroscience*, 35(5):2161–2172.
- 633 Bharadwaj, H. M., Verhulst, S., Shaheen, L., Liberman, M. C., and Shinn-
634 Cunningham, B. G. (2014). Cochlear neuropathy and the coding of supra-
635 threshold sound. *Frontiers in systems neuroscience*, 8:26.
- 636 Bourien, J., Tang, Y., Batrel, C., Huet, A., Lenoir, M., Ladrech, S., Des-
637 madryl, G., Nouvian, R., Puel, J.-L., and Wang, J. (2014). Contribution
638 of auditory nerve fibers to compound action potential of the auditory nerve.
639 *Journal of neurophysiology*, 112(5):1025–1039.

- 640 Bramhall, N. F., Konrad-Martin, D., McMillan, G. P., and Griest, S. E.
641 (2017). Auditory brainstem response altered in humans with noise expo-
642 sure despite normal outer hair cell function. *Ear and hearing*, 38(1):e1.
- 643 Buzsaki, G. (2006). *Rhythms of the Brain*, chapter Perceptions and Actions
644 Are Brain-State Dependent. Oxford University Press.
- 645 Coughlin, S. S. (1990). Recall bias in epidemiologic studies. *Journal of*
646 *clinical epidemiology*, 43(1):87–91.
- 647 Degeest, S., Corthals, P., Vinck, B., and Keppler, H. (2014). Prevalence
648 and characteristics of tinnitus after leisure noise exposure in young adults.
649 *NOISE and HEALTH*, 16(68):26–33.
- 650 Don, M. and Eggermont, J. (1978). Analysis of the click-evoked brainstem
651 potentials in man using high-pass noise masking. *The journal of the a*
652 *stical society of America*, 63(4):1084–1092.
- 653 Eggermont, J. (1976). Analysis of compound action potential responses to
654 tone bursts in the human and guinea pig cochlea. *The Journal of the*
655 *Acoustical Society of America*, 60(5):1132–1139.
- 656 Encina-Llamas, G., Harte, J. M., Dau, T., Shinn-Cunningham, B., and Epp,
657 B. (2019). Investigating the effect of cochlear synaptopathy on envelope
658 following responses using a model of the auditory nerve. *Journal of the*
659 *Association for Research in Otolaryngology*, pages 1–20.
- 660 Fernandez, K. A., Jeffers, P. W., Lall, K., Liberman, M. C., and Kujawa,
661 S. G. (2015). Aging after noise exposure: acceleration of cochlear synap-
662 topathy in “recovered” ears. *Journal of Neuroscience*, 35(19):7509–7520.

663 Furman, A. C., Kujawa, S. G., and Liberman, M. C. (2013). Noise-induced
664 cochlear neuropathy is selective for fibers with low spontaneous rates. *Jour-*
665 *nal of neurophysiology*, 110(3):577–586.

666 Garrett, M. and Verhulst, S. (2019). Applicability of subcortical eeg metrics
667 of synaptopathy to older listeners with impaired audiograms. *Hearing*
668 *research*, 380:150–165.

669 Gorga, M. P., Worthington, D. W., Reiland, J. K., Beauchaine, K. A., and
670 Goldgar, D. E. (1985). Some comparisons between auditory brain stem
671 response thresholds, latencies, and the pure-tone audiogram. *Ear and*
672 *Hearing*, 6(2):105–112.

673 Greenwood, D. D. (1990). A cochlear frequency-position function for several
674 species—29 years later. *The Journal of the Acoustical Society of America*,
675 87(6):2592–2605.

676 Guest, H., Munro, K. J., Prendergast, G., Millman, R. E., and Plack, C. J.
677 (2018). Impaired speech perception in noise with a normal audiogram:
678 No evidence for cochlear synaptopathy and no relation to lifetime noise
679 exposure. *Hearing research*, 364:142–151.

680 Joris, P. X. and Yin, T. C. (1992). Responses to amplitude-modulated tones
681 in the auditory nerve of the cat. *The Journal of the Acoustical Society of*
682 *America*, 91(1):215–232.

683 Keshishzadeh, S., Vasilkov, V., and Verhulst, S. (2019). Tonotopic sensitiv-
684 ity to supra-threshold hearing deficits of the envelope following response

- 685 evoked by broadband stimuli. In *23rd International Congress on Acoustics*
686 (*ICA 2019*), pages 6513–6518.
- 687 Kujawa, S. G. and Liberman, M. C. (2009). Adding insult to injury: cochlear
688 nerve degeneration after “temporary” noise-induced hearing loss. *Journal*
689 *of Neuroscience*, 29(45):14077–14085.
- 690 Kummer, P., Janssen, T., and Arnold, W. (1998). The level and growth
691 behavior of the 2 f₁- f₂ distortion product otoacoustic emission and its
692 relationship to auditory sensitivity in normal hearing and cochlear hearing
693 loss. *The Journal of the Acoustical Society of America*, 103(6):3431–3444.
- 694 Liberman, M. C. (1978). Auditory-nerve response from cats raised in a
695 low-noise chamber. *The Journal of the Acoustical Society of America*,
696 63(2):442–455.
- 697 Liberman, M. C. and Kujawa, S. G. (2017). Cochlear synaptopathy in ac-
698 quired sensorineural hearing loss: Manifestations and mechanisms. *Hearing*
699 *research*, 349:138–147.
- 700 Lin, H. W., Furman, A. C., Kujawa, S. G., and Liberman, M. C. (2011).
701 Primary neural degeneration in the guinea pig cochlea after reversible
702 noise-induced threshold shift. *Journal of the Association for Research in*
703 *Otolaryngology*, 12(5):605–616.
- 704 Liu, L., Wang, H., Shi, L., Almklass, A., He, T., Aiken, S., Bance, M.,
705 Yin, S., and Wang, J. (2012). Silent damage of noise on cochlear afferent
706 innervation in guinea pigs and the impact on temporal processing. *PLoS*
707 *One*, 7(11):e49550.

- 708 Lobarinas, E., Spankovich, C., and Le Prell, C. G. (2017). Evidence of
709 “hidden hearing loss” following noise exposures that produce robust tts
710 and abr wave-i amplitude reductions. *Hearing research*, 349:155–163.
- 711 Long, G. R., Talmadge, C. L., and Lee, J. (2008). Measuring distortion
712 product otoacoustic emissions using continuously sweeping primaries. *The*
713 *Journal of the Acoustical Society of America*, 124(3):1613–1626.
- 714 Makary, C. A., Shin, J., Kujawa, S. G., Liberman, M. C., and Merchant,
715 S. N. (2011). Age-related primary cochlear neuronal degeneration in human
716 temporal bones. *Journal of the Association for Research in Otolaryngology*,
717 12(6):711–717.
- 718 Mauermann, M. (2013). Improving the usability of the distortion product
719 otoacoustic emissions (dpoae)-sweep method: An alternative artifact re-
720 jection and noise-floor estimation. In *Proceedings of Meetings on Acoustics*
721 *ICA2013*, volume 19, page 050054. ASA.
- 722 Mehraei, G., Hickox, A. E., Bharadwaj, H. M., Goldberg, H., Verhulst, S.,
723 Liberman, M. C., and Shinn-Cunningham, B. G. (2016). Auditory brain-
724 stem response latency in noise as a marker of cochlear synaptopathy. *Jour-*
725 *nal of Neuroscience*, 36(13):3755–3764.
- 726 Mitchell, C., Phillips, D. S., and Trune, D. R. (1989). Variables affecting
727 the auditory brainstem response: audiogram, age, gender and head size.
728 *Hearing research*, 40(1-2):75–85.
- 729 Moore, B. C. and Glasberg, B. R. (1983). Suggested formulae for calculating

- 730 auditory-filter bandwidths and excitation patterns. *The journal of the*
731 *acoustical society of America*, 74(3):750–753.
- 732 Parthasarathy, A. and Kujawa, S. G. (2018). Synaptopathy in the aging
733 cochlea: Characterizing early-neural deficits in auditory temporal envelope
734 processing. *Journal of Neuroscience*, 38(32):7108–7119.
- 735 Picton, T. W. (2010). *Human auditory evoked potentials*. Plural Publishing.
- 736 Plack, C. J., Léger, A., Prendergast, G., Kluk, K., Guest, H., and Munro,
737 K. J. (2016). Toward a diagnostic test for hidden hearing loss. *Trends in*
738 *hearing*, 20:2331216516657466.
- 739 Prendergast, G., Guest, H., Munro, K. J., Kluk, K., Léger, A., Hall, D. A.,
740 Heinz, M. G., and Plack, C. J. (2017). Effects of noise exposure on young
741 adults with normal audiograms i: Electrophysiology. *Hearing research*,
742 344:68–81.
- 743 Purcell, D. W., John, S. M., Schneider, B. A., and Picton, T. W. (2004). Hu-
744 man temporal auditory acuity as assessed by envelope following responses.
745 *The Journal of the Acoustical Society of America*, 116(6):3581–3593.
- 746 Rasetshwane, D. M., Argenyi, M., Neely, S. T., Kopun, J. G., and Gorga,
747 M. P. (2013). Latency of tone-burst-evoked auditory brain stem responses
748 and otoacoustic emissions: Level, frequency, and rise-time effects. *The*
749 *Journal of the Acoustical Society of America*, 133(5):2803–2817.
- 750 Shaheen, L. A., Valero, M. D., and Liberman, M. C. (2015). Towards a di-
751 agnosis of cochlear neuropathy with envelope following responses. *Journal*
752 *of the Association for Research in Otolaryngology*, 16(6):727–745.

- 753 Trune, D. R., Mitchell, C., and Phillips, D. S. (1988). The relative importance
754 of head size, gender and age on the auditory brainstem response. *Hearing*
755 *research*, 32(2-3):165–174.
- 756 Valero, M., Burton, J., Hauser, S., Hackett, T., Ramachandran, R., and
757 Liberman, M. (2017). Noise-induced cochlear synaptopathy in rhesus mon-
758 keys (*macaca mulatta*). *Hearing research*, 353:213–223.
- 759 Vasilkov, V. and Verhulst, S. (2019). Towards a differential diagnosis of
760 cochlear synaptopathy and outer-hair-cell deficits in mixed sensorineural
761 hearing loss pathologies. *medRxiv*.
- 762 Verhulst, S., Altoe, A., and Vasilkov, V. (2018a). Computational model-
763 ing of the human auditory periphery: Auditory-nerve responses, evoked
764 potentials and hearing loss. *Hearing research*, 360:55–75.
- 765 Verhulst, S., Ernst, F., Garrett, M., and Vasilkov, V. (2018b). Suprathresh-
766 old psychoacoustics and envelope-following response relations: Normal-
767 hearing, synaptopathy and cochlear gain loss. *Acta Acustica united with*
768 *Acustica*, 104(5):800–803.
- 769 Verhulst, S., Jagadeesh, A., Mauermann, M., and Ernst, F. (2016). In-
770 dividual differences in auditory brainstem response wave characteristics:
771 relations to different aspects of peripheral hearing loss. *Trends in hearing*,
772 20:2331216516672186.
- 773 Viana, L. M., O'Malley, J. T., Burgess, B. J., Jones, D. D., Oliveira, C. A.,
774 Santos, F., Merchant, S. N., Liberman, L. D., and Liberman, M. C. (2015).

- 775 Cochlear neuropathy in human presbycusis: Confocal analysis of hidden
776 hearing loss in post-mortem tissue. *Hearing research*, 327:78–88.
- 777 Wu, P., Liberman, L., Bennett, K., De Gruttola, V., O'Malley, J., and Liber-
778 man, M. (2019). Primary neural degeneration in the human cochlea: evi-
779 dence for hidden hearing loss in the aging ear. *Neuroscience*, 407:8–20.
- 780 Zhu, L., Bharadwaj, H., Xia, J., and Shinn-Cunningham, B. (2013). A
781 comparison of spectral magnitude and phase-locking value analyses of the
782 frequency-following response to complex tones. *The Journal of the Acous-
783 tical Society of America*, 134(1):384–395.

784 **Figure Captions**

Figure 1. Measured audiograms in the first (left) and second (right) experiment. Markers indicate the audiometric threshold at 4 kHz. The dashed line is the averaged audiometric threshold at each group and the yellow shading the standard deviation.

Figure 2. Spectra of the 120-Hz modulated stimuli and derived bands. (a) Designed stimulus spectra in different frequency bands and specified cut-off frequencies of the bandpass filter. (b) Derived bands from the EFRs recorded to the stimuli shown in (a) obtained by spectral subtraction.

Figure 3. Modeling approach. The block-diagram shows different levels of the auditory pathway modelled in the employed biophysical model of the hearing periphery (Verhulst et al., 2018a). The top-right graph indicates the simulated distribution of different types of AN fibers across CF. The table shows simulated CS profiles and the graph on the bottom right depicts simulated different degrees of cochlear gain loss. The corresponding simulated thresholds at 8 kHz are indicated by the legend.

Figure 4. EFR_{PtN} magnitudes to 120-Hz modulated stimuli with different white noise carrier bandwidths in the (a) first and (b) second experiment. Individual data-points are depicted with open symbols and standard deviations were obtained using a bootstrapping procedure (Zhu et al., 2013).

Filled symbols reflect the group-means and their corresponding standard deviations. Simulated EFRs from a NH model were added in filled hexagons.

Figure 5. $\text{DBEFR}_{\text{PtN}}$ magnitudes derived using Eq. 3 for 120 Hz modulated stimuli with different white-noise-carrier bandwidths in the (a) first and (b) second experiment. $\text{DBEFR}_{\text{PtN}}$ for each frequency band was obtained from a wider and narrower width stimulus. Standard deviations were calculated using a bootstrapping procedure and stemmed from averaged responses from 20 stimulus iterations in the model simulations. Group means and standard deviations are depicted using filled symbols.

Figure 6. Correlation analysis of $\text{EFR}_{[2-22]}$ ($\text{EFR}_{[2.828-16]}$) with age, audiometric threshold at 4 kHz, head-size and DPTH_{3000} (DPTH_{4000}) in the first (left) and second (right) experiments.

Figure 7. Correlation analysis of $\text{DBEFR}_{[2-4]}$ ($\text{DBEFR}_{[2.828-5.656]}$) with age, audiometric threshold at 4 kHz, head-size and DPTH_{3000} (DPTH_{4000}) in the first (left) and second (right) experiments.

Figure 8. Bar-plots of noise scores acquired from questionnaires of NH and NHR groups, classified in three categories, i.e. experience noise as a consequence of (i) playing a musical instrument in a band, (ii) attending festivals or concerts and (iii) using noisy tools. Noise scores with high values are colored in orange and can be compared to the corresponding individual $\text{DBEFR}_{[2-4]}$ magnitudes of (a) NH and (b) NHR listeners. Results are shown normalised,

where the score of 1 corresponds to 30600, 18480 and 26000 hours of accumulated noise dose on the considered categories, respectively.

Figure 9. Experimental EFR_{PtN} and $\text{DBEFR}_{\text{PtN}}$ magnitudes (colored open symbols): (a) EFR_{PtN} to [2-22] and [4-22] kHz, (b) EFRs to [2.828-16] and [5.656-16] kHz and (c) DBEFRs at [2-4] kHz and (d) DBEFRs at [2.828-5.656] kHz. Simulated EFR_{PtN} (a,b) and $\text{DBEFR}_{\text{PtN}}$ (c,d) magnitudes are shown in each panel using filled hexagons and degrees of CS as indicated on the X axis and CF-dependent patterns of OHC damage as given by the legend.

Figure 10. Modulated responses calculated at each CF using Eq. 6 and 7 to different experimental conditions for normal listeners and different sensorineural hearing losses at the AN processing level of the model, (a) broadband and (b) derived-band. In both panels, dotted lines show AN-responses to sloping 10 dB-HL OHC-loss at 8 kHz and lighter colors indicate AN responses to certain degree of CS.

785 **Figures**

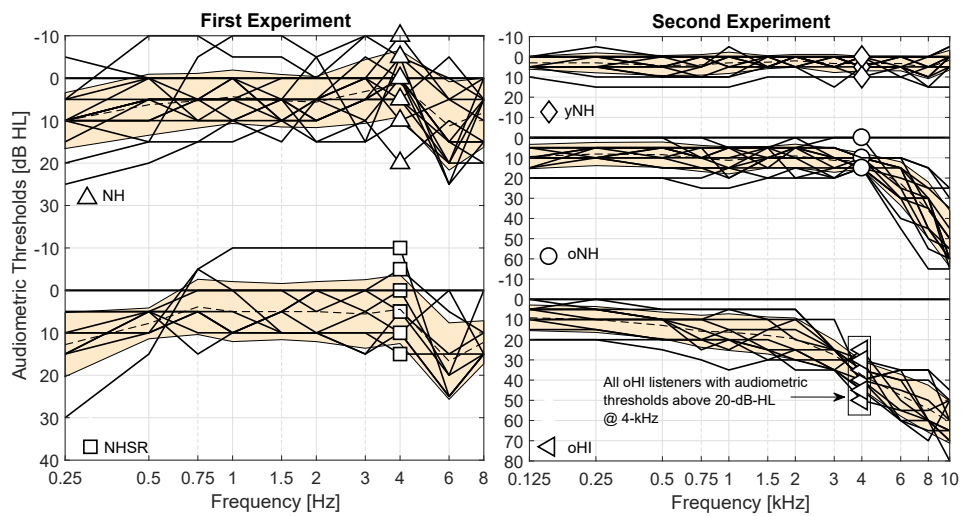


Figure 1

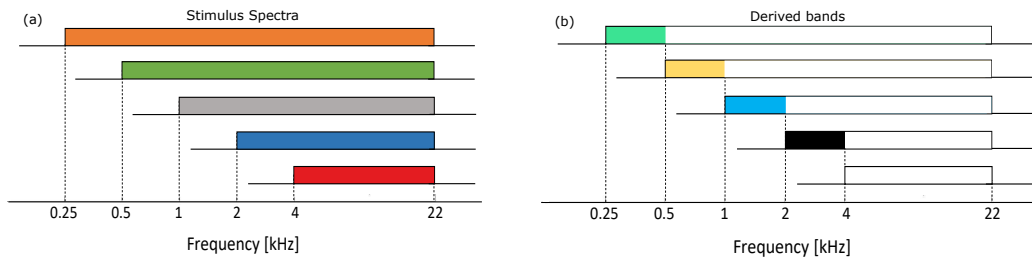


Figure 2

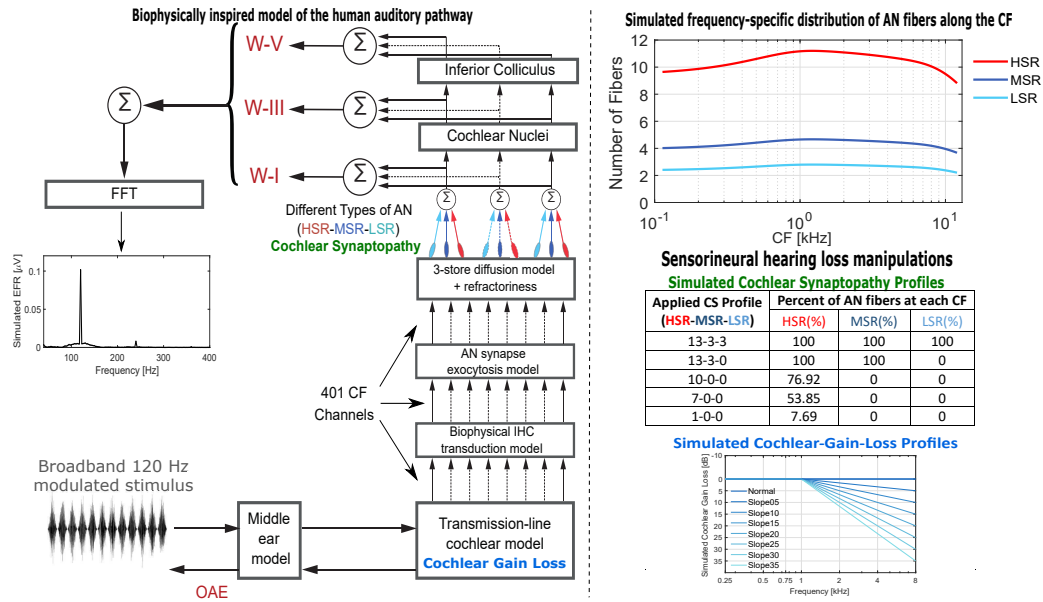


Figure 3

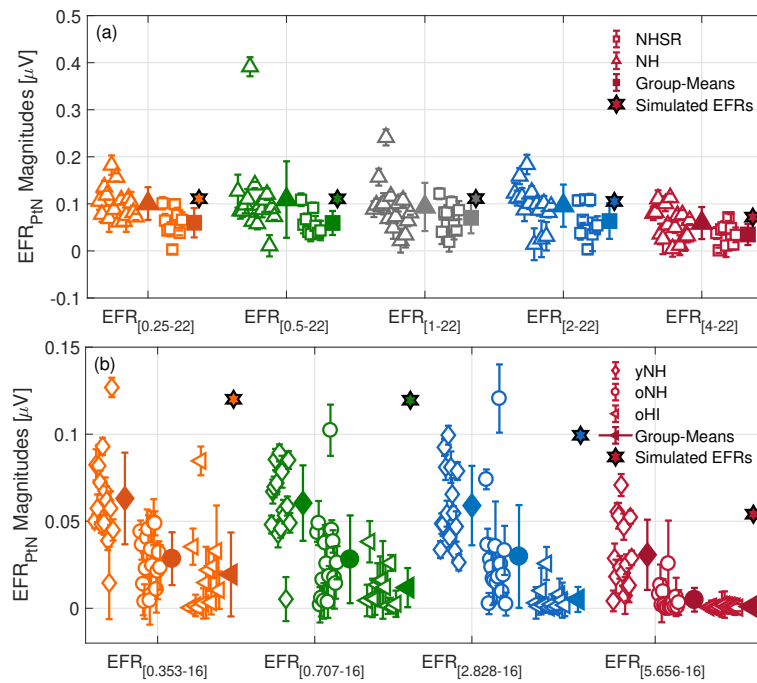


Figure 4

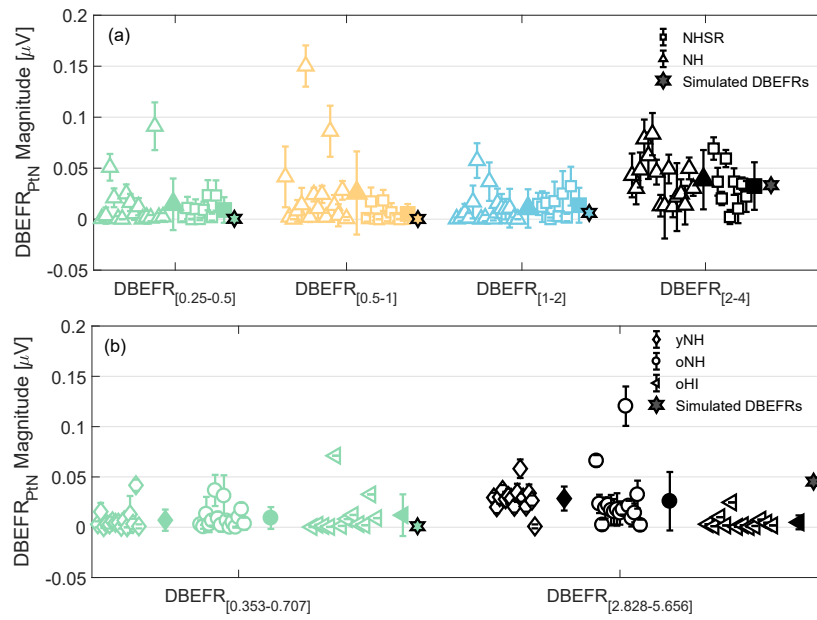


Figure 5

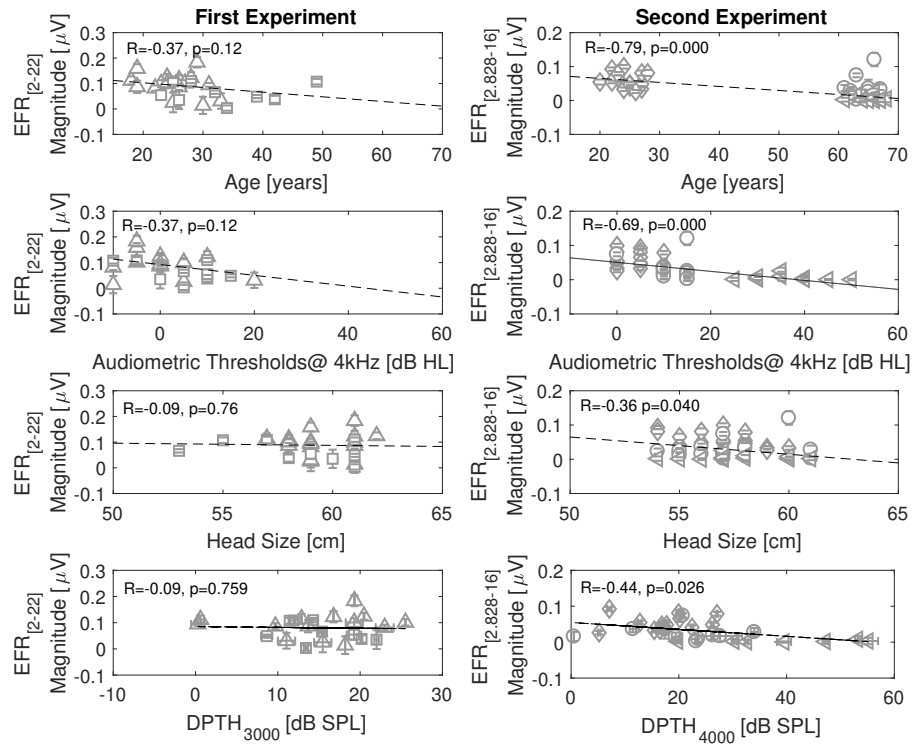


Figure 6

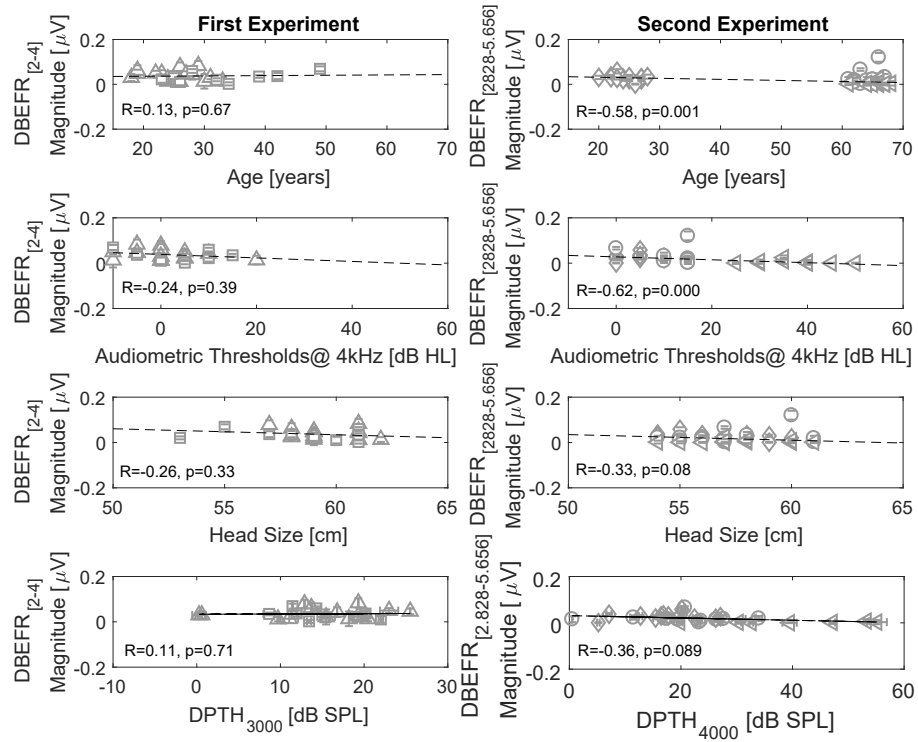


Figure 7

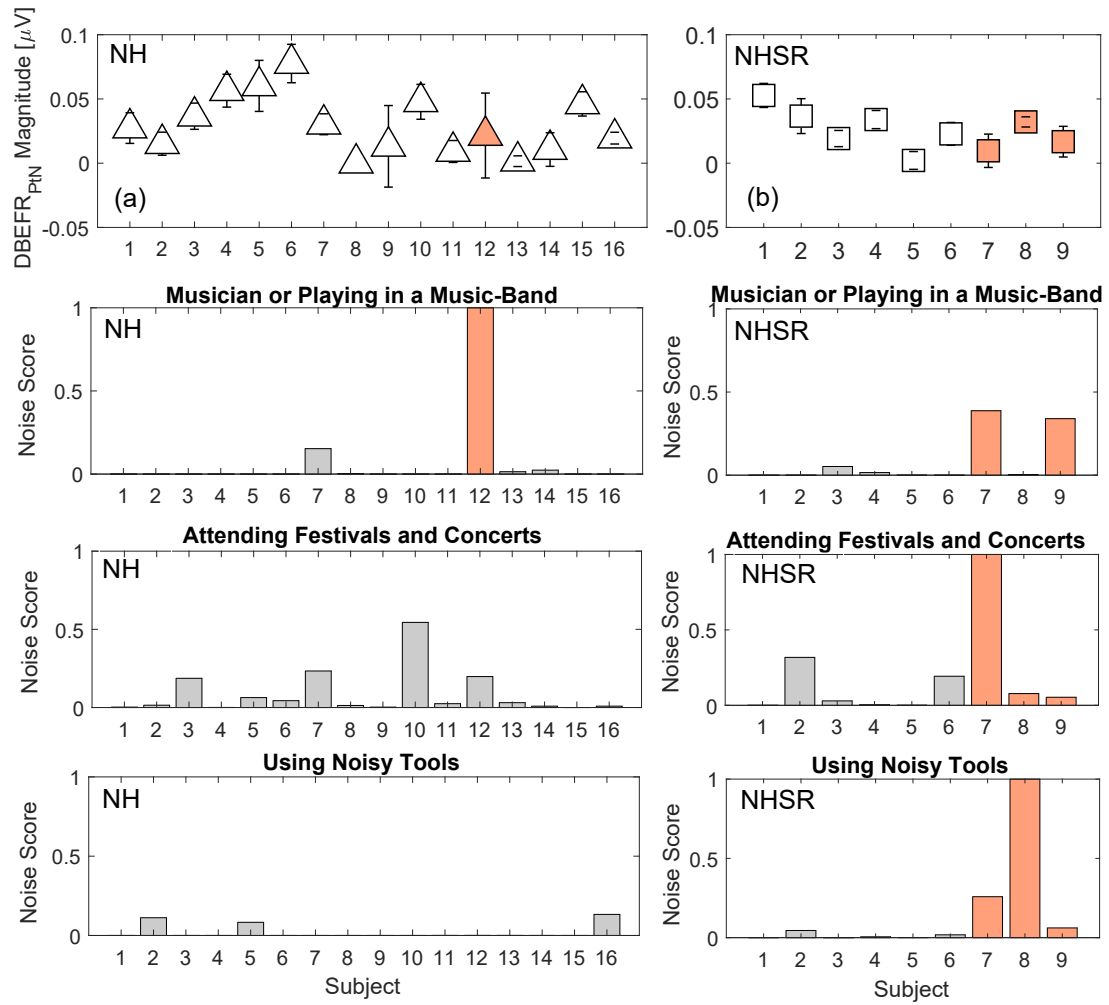


Figure 8

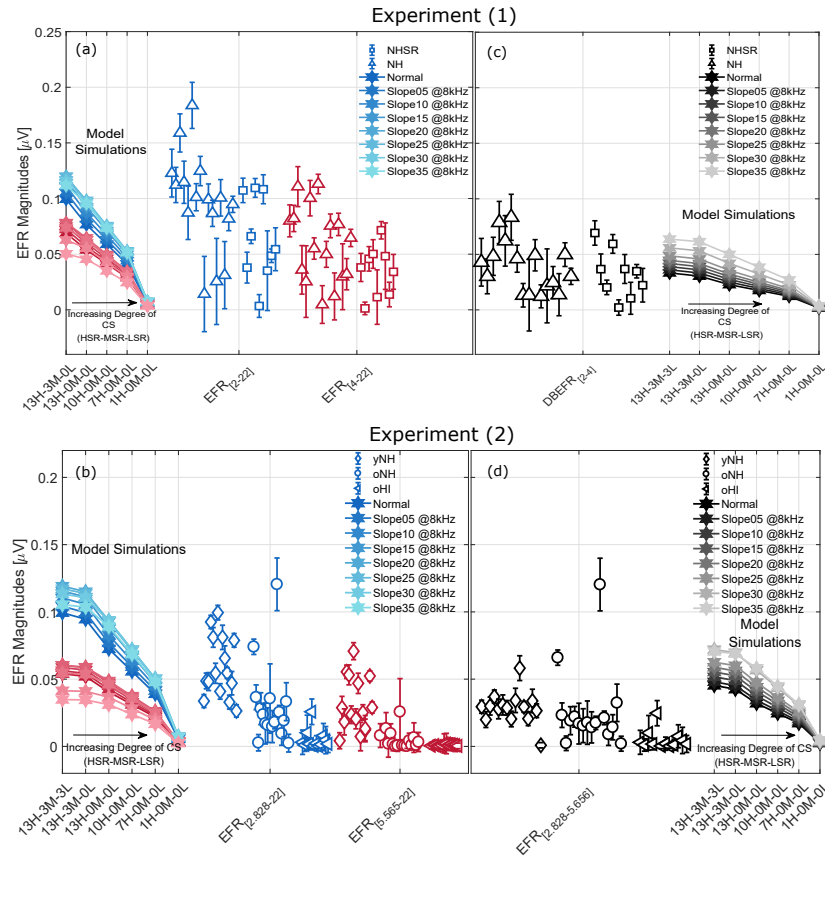


Figure 9

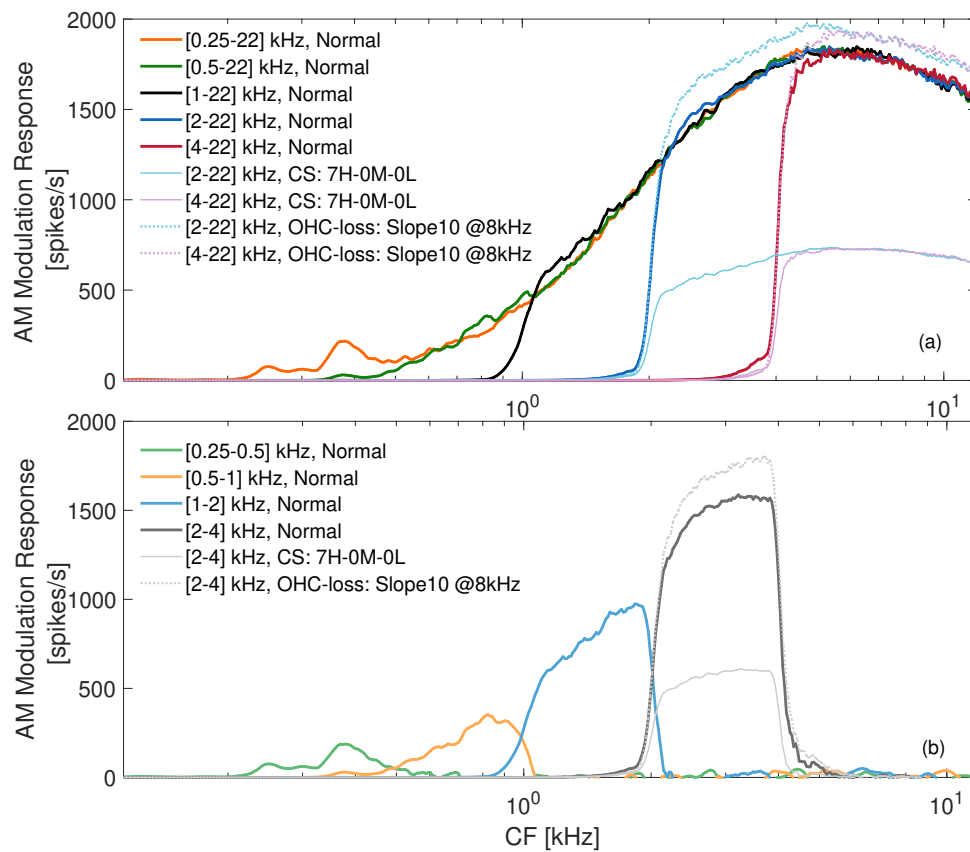
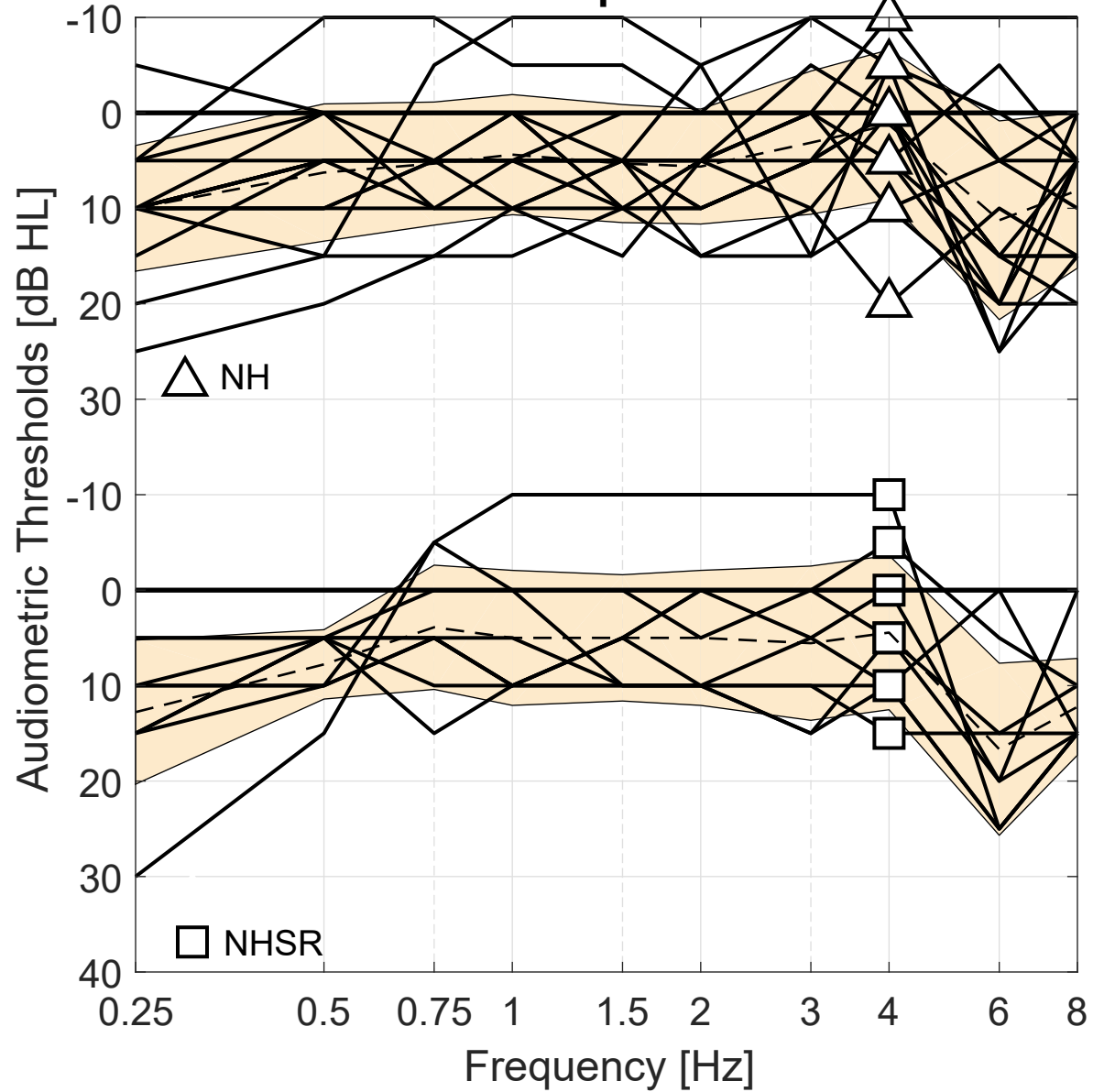
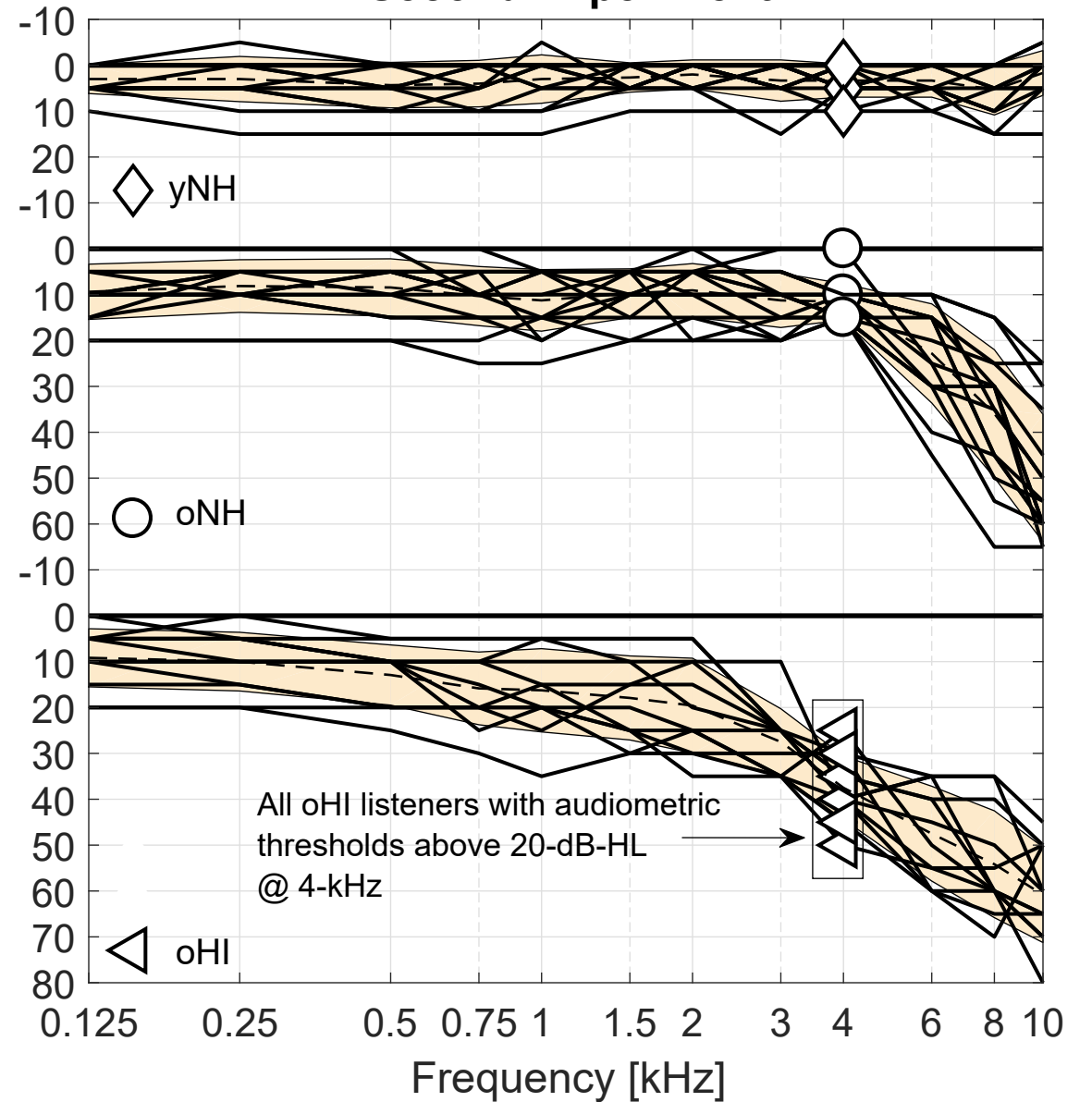


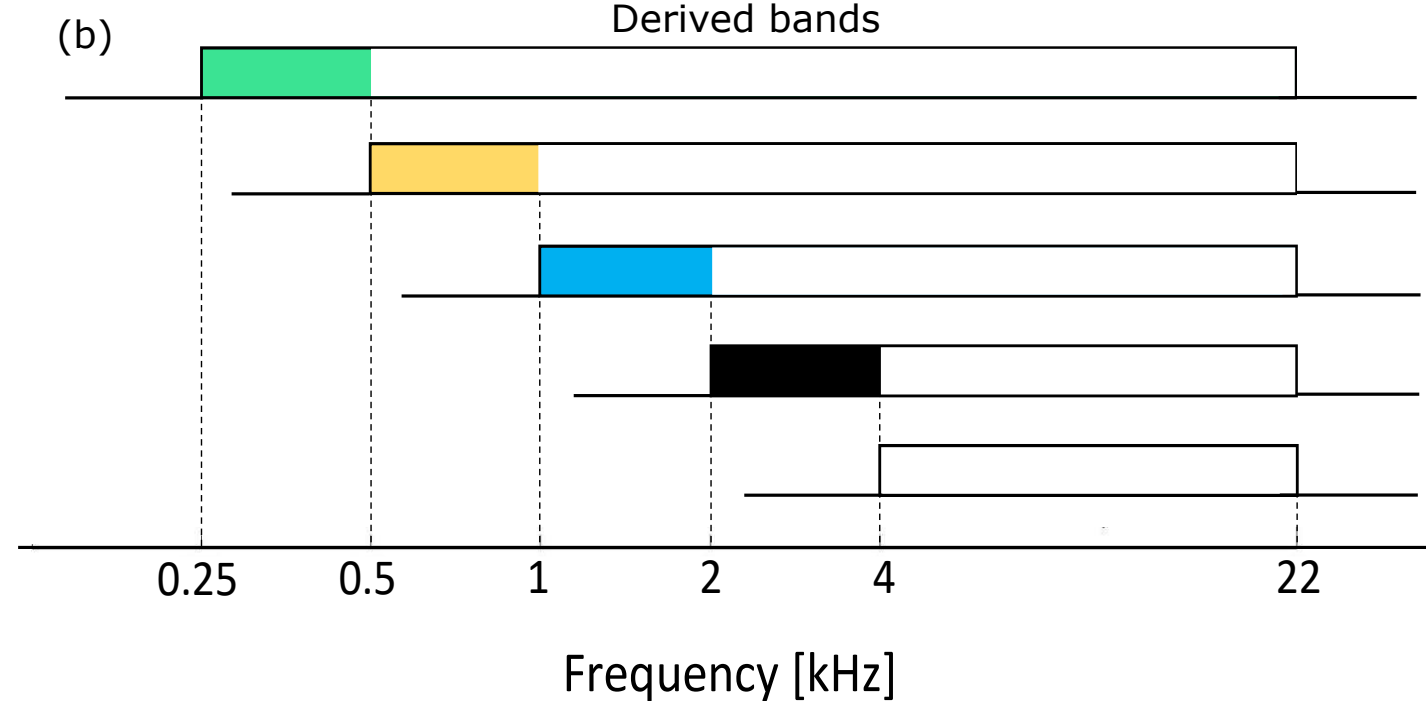
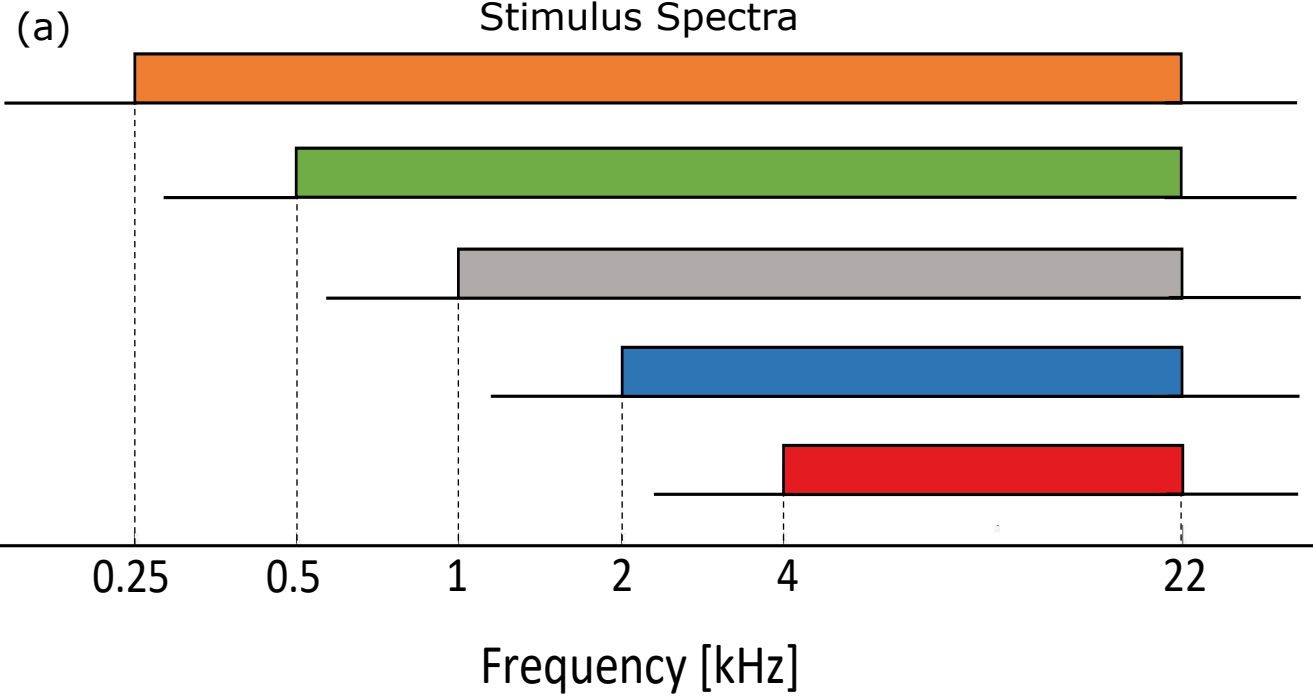
Figure 10

First Experiment

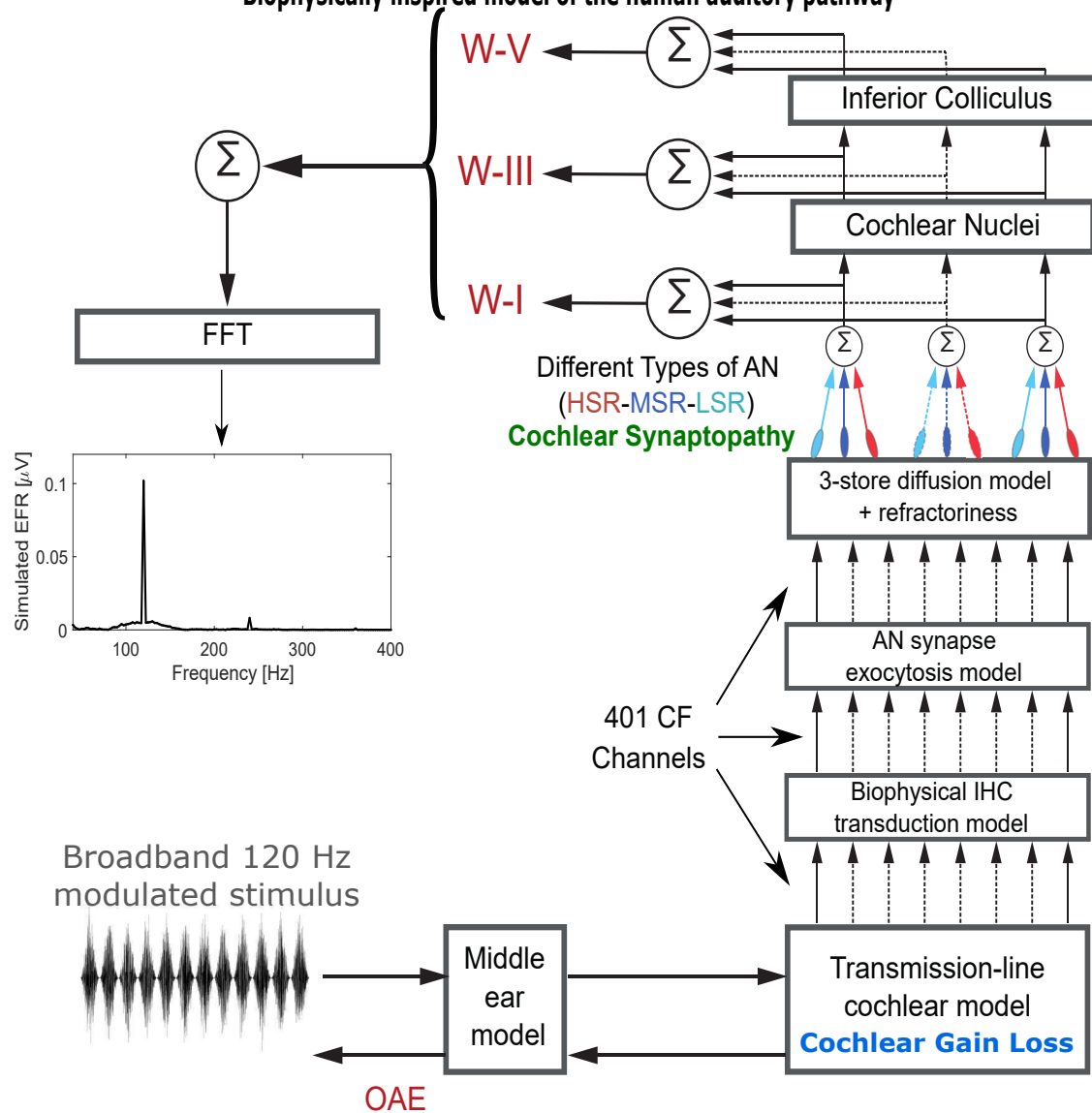


Second Experiment

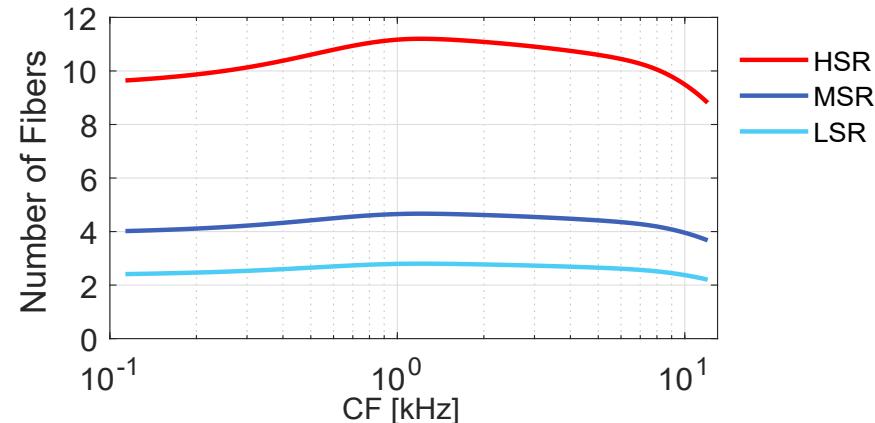




Biophysically inspired model of the human auditory pathway



Simulated frequency-specific distribution of AN fibers along the CF

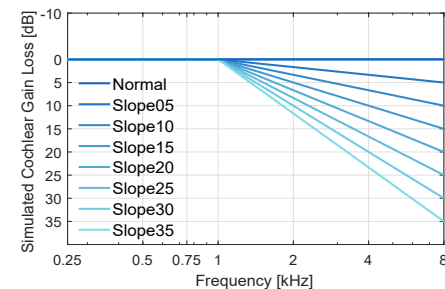


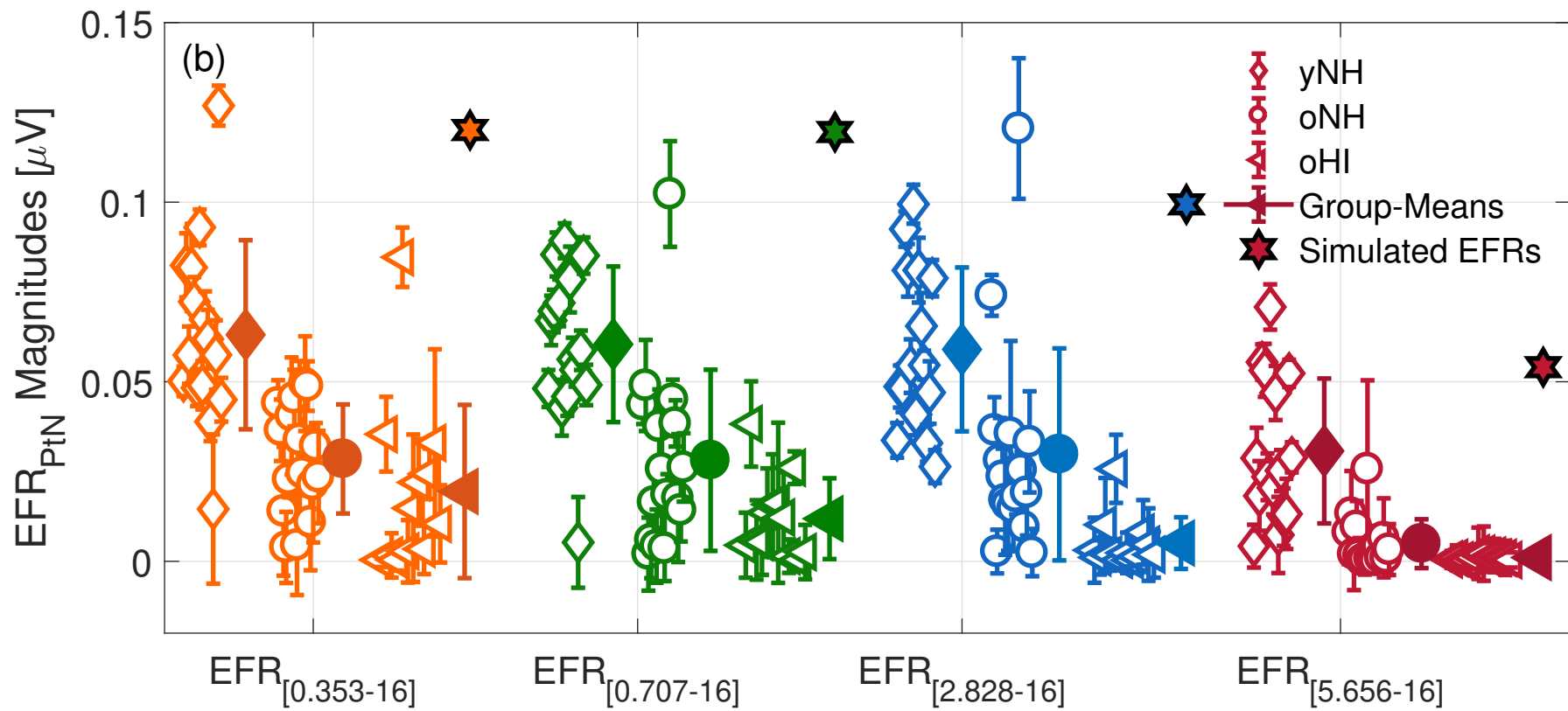
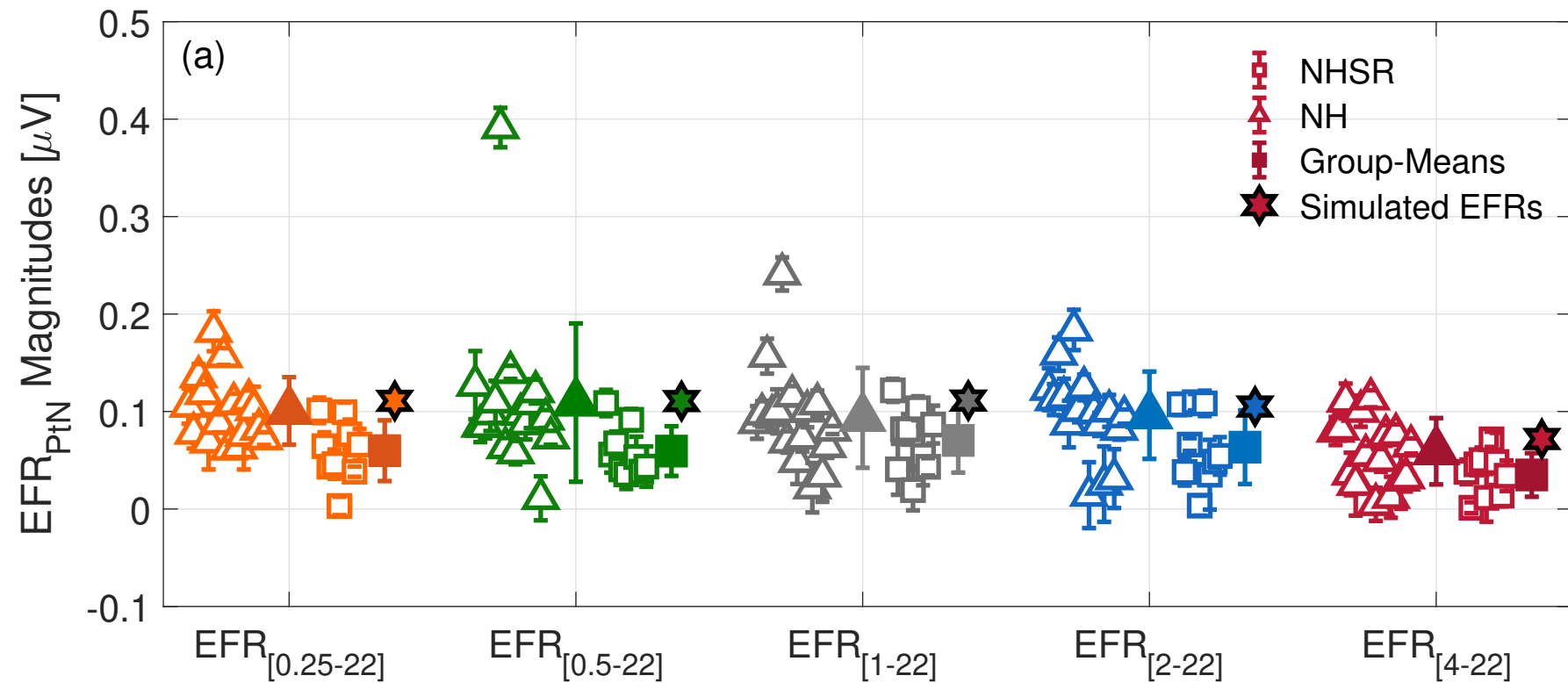
Sensorineural hearing loss manipulations

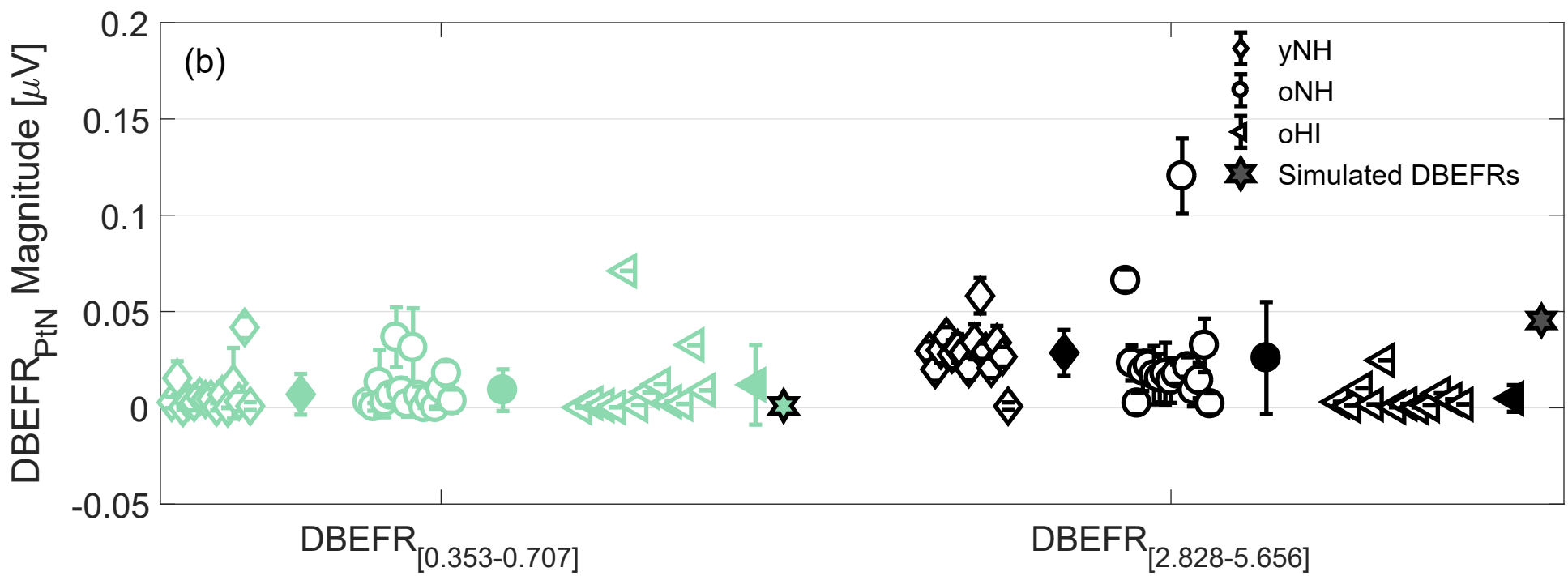
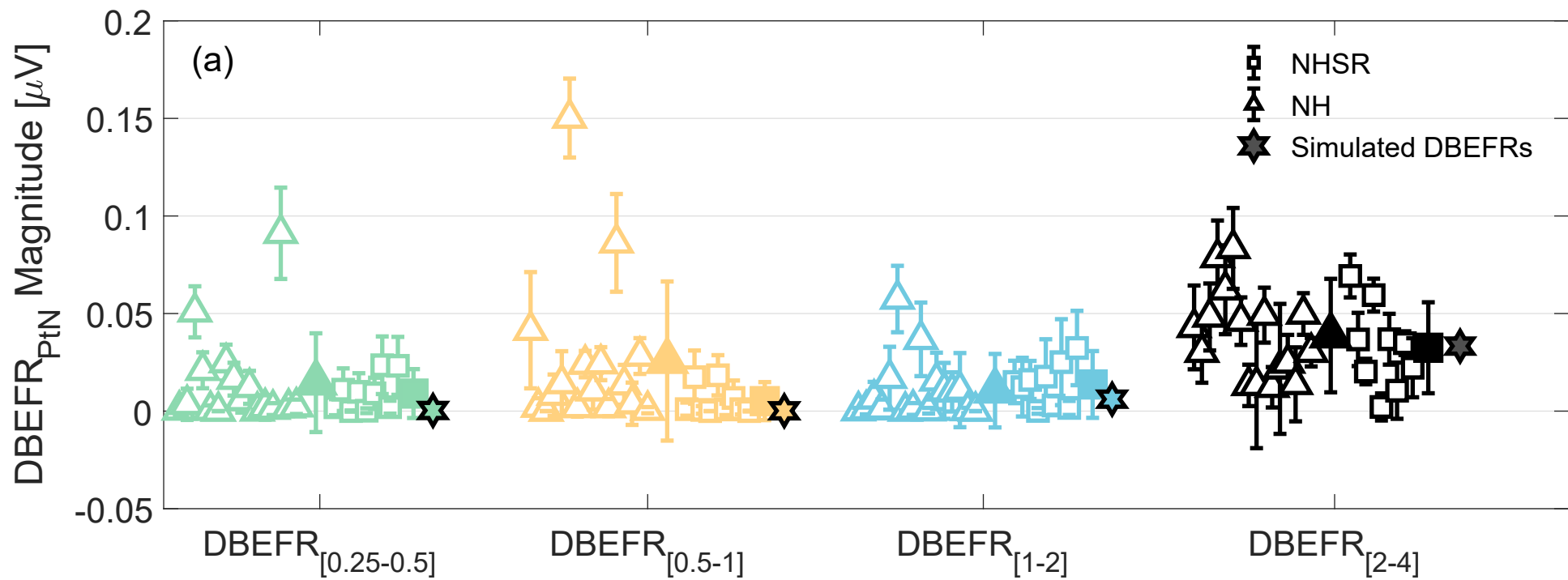
Simulated Cochlear Synaptopathy Profiles

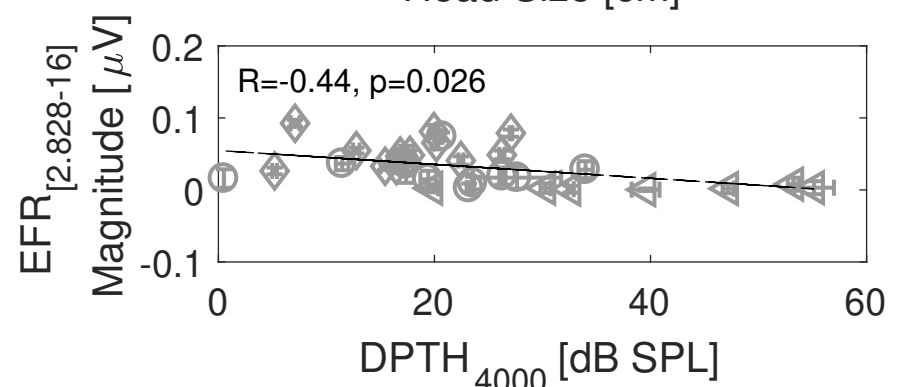
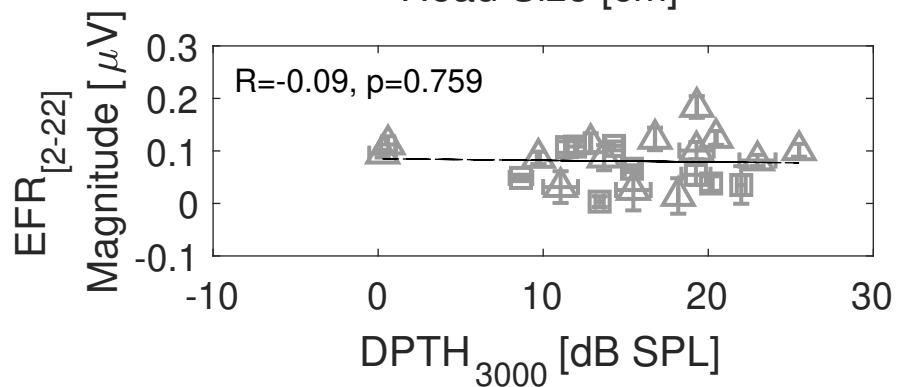
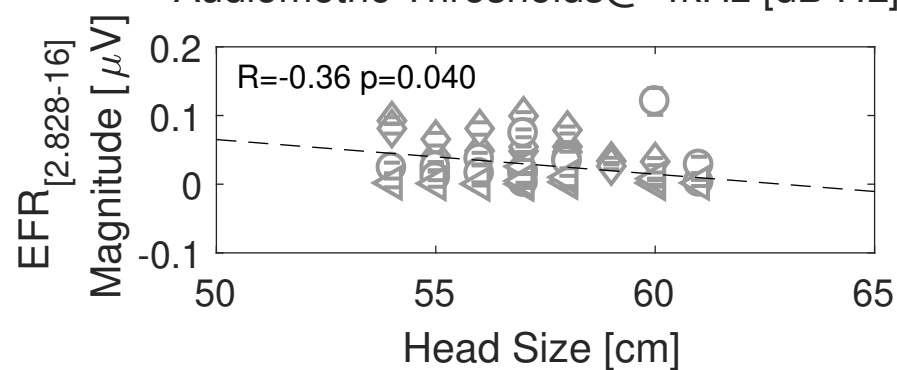
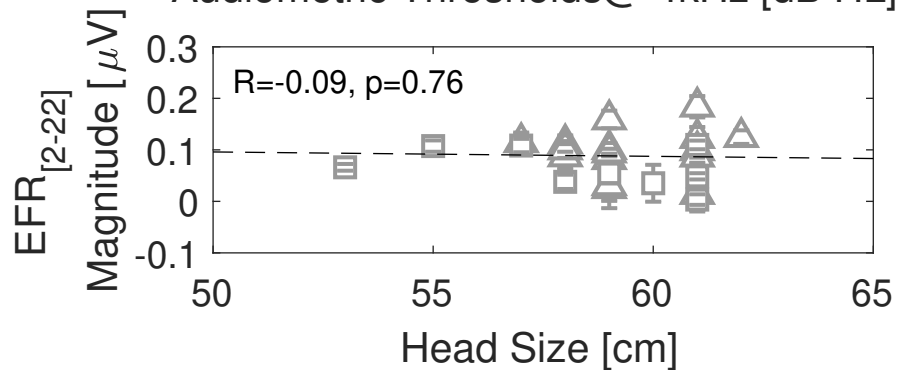
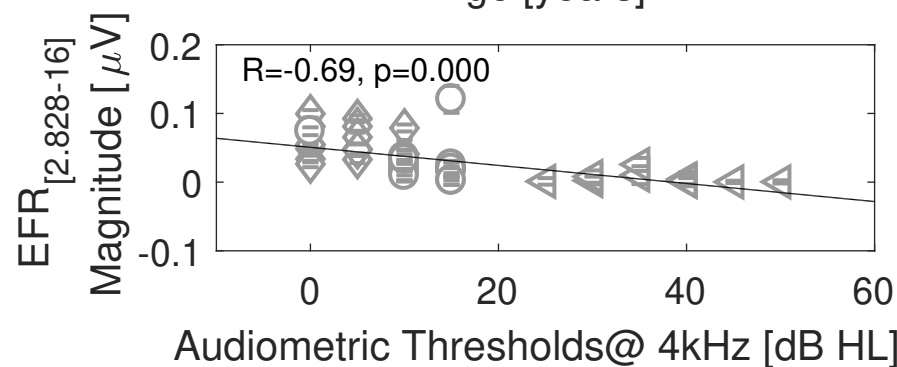
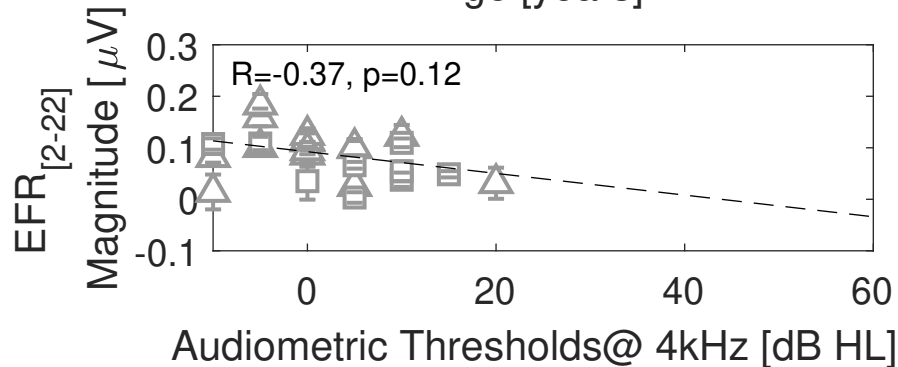
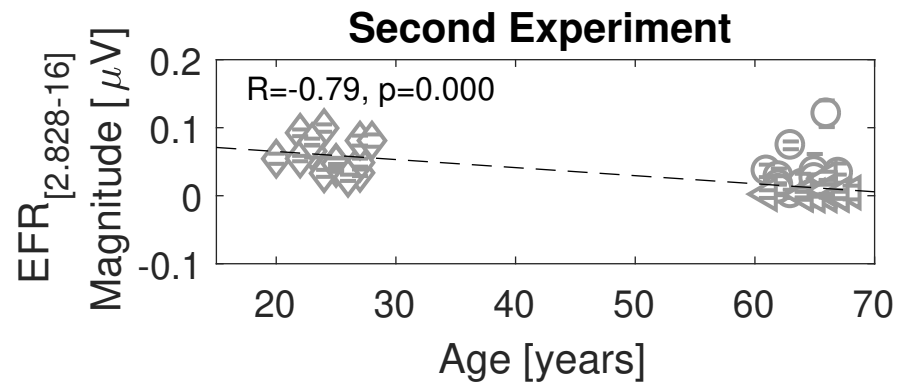
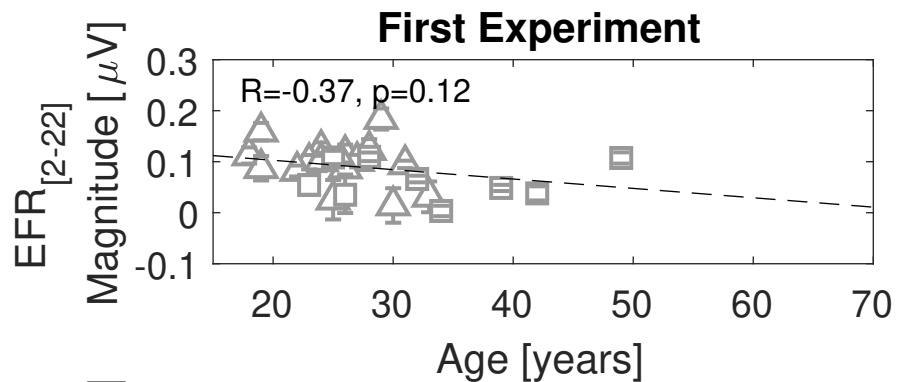
Applied CS Profile (HSR-MSR-LSR)	Percent of AN fibers at each CF		
	HSR(%)	MSR(%)	LSR(%)
13-3-3	100	100	100
13-3-0	100	100	0
10-0-0	76.92	0	0
7-0-0	53.85	0	0
1-0-0	7.69	0	0

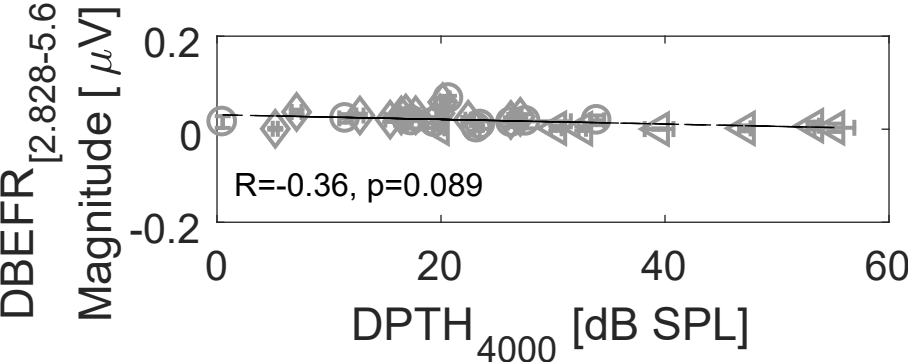
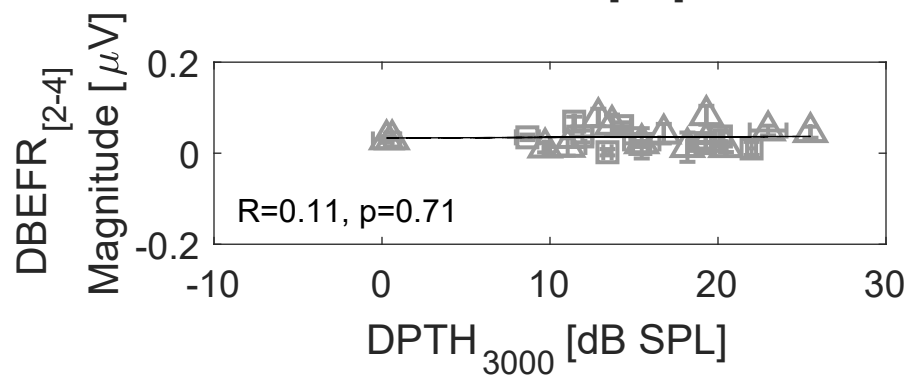
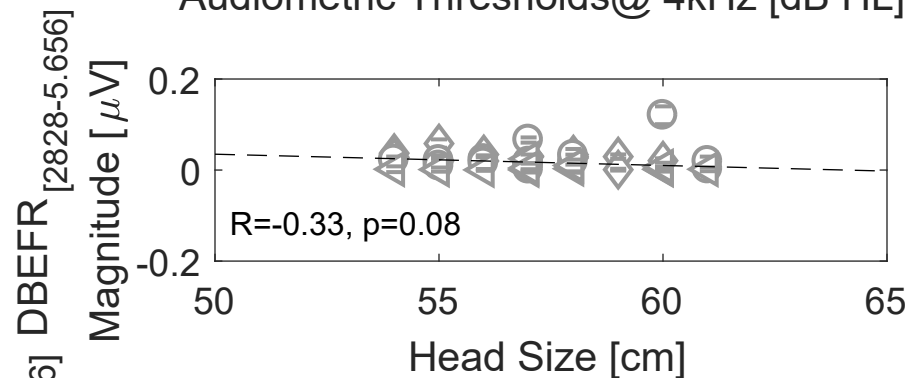
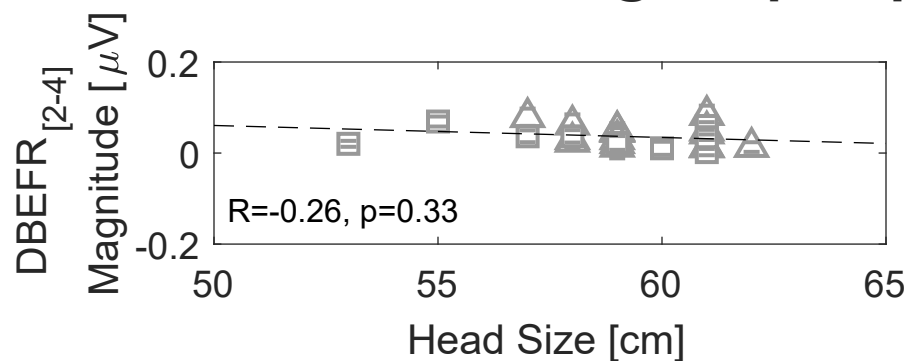
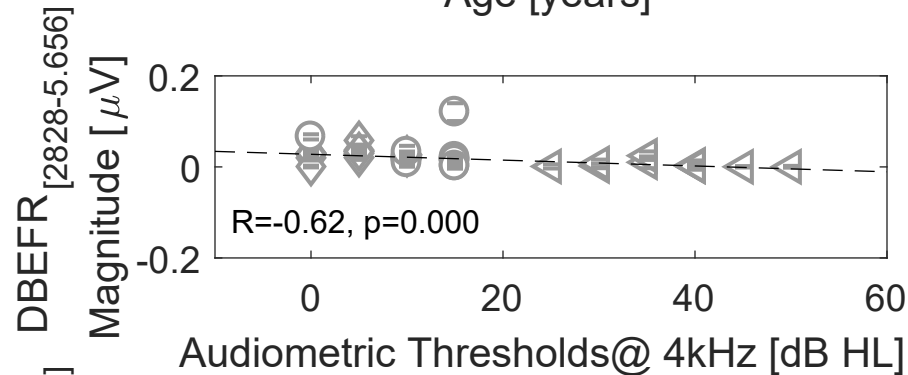
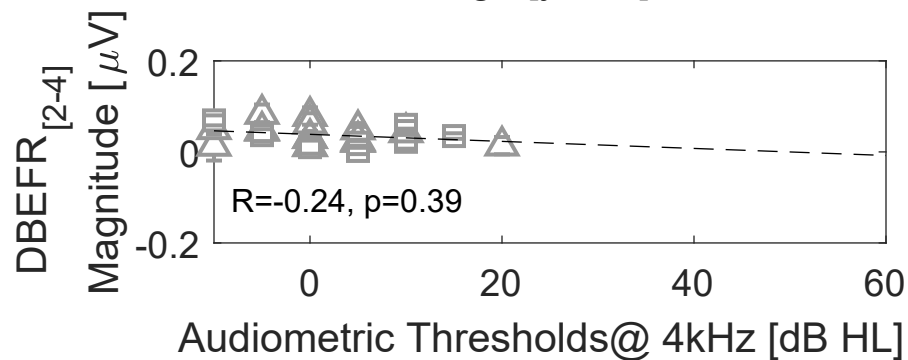
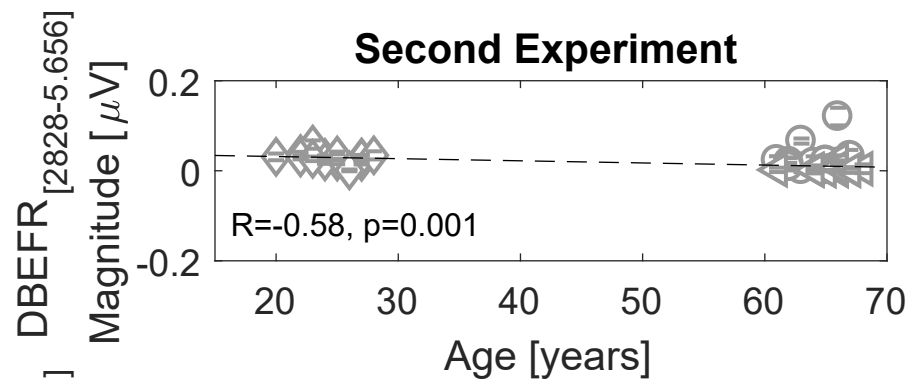
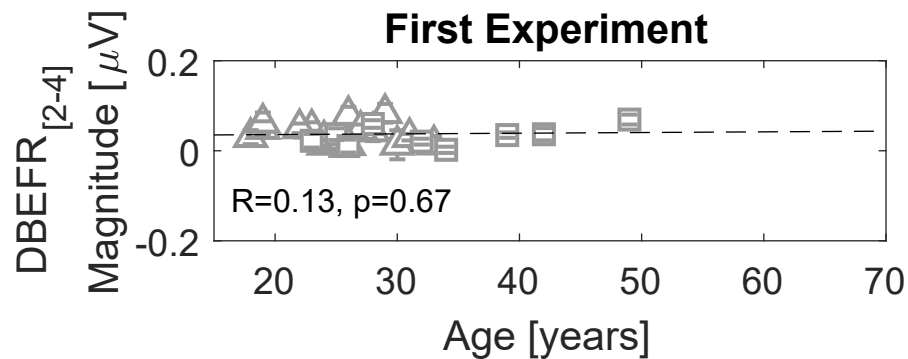
Simulated Cochlear-Gain-Loss Profiles

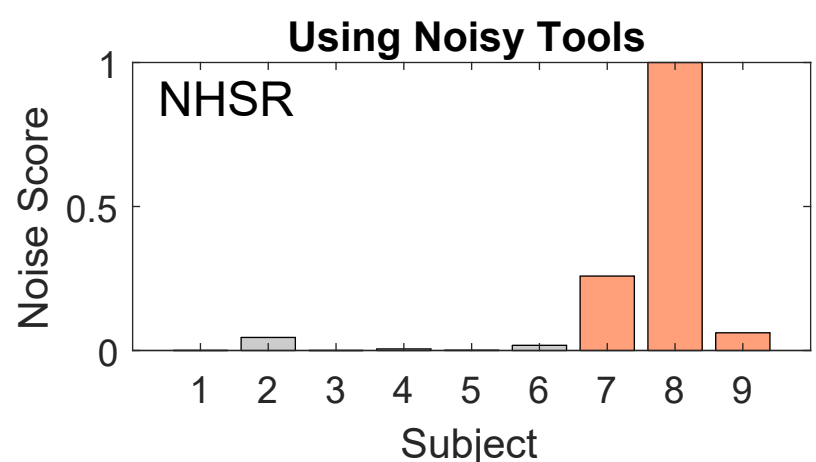
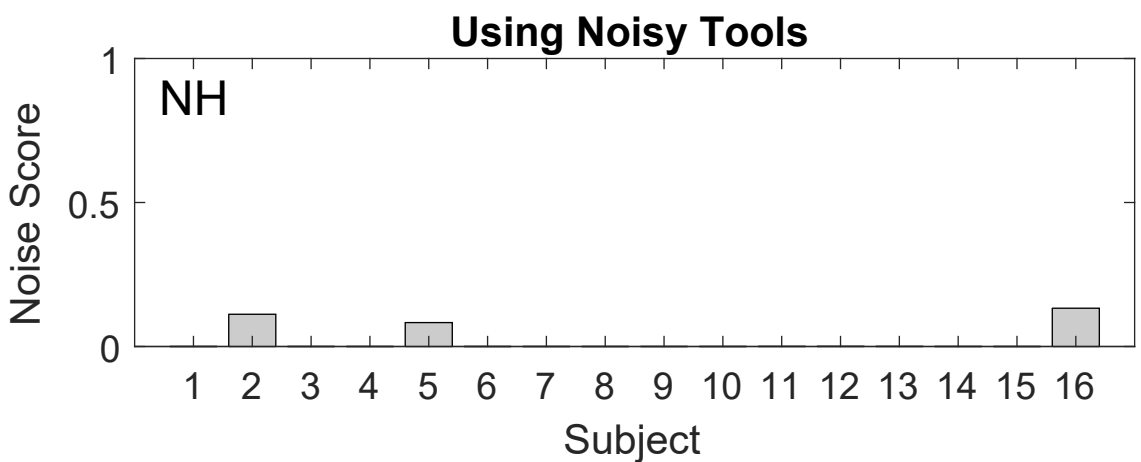
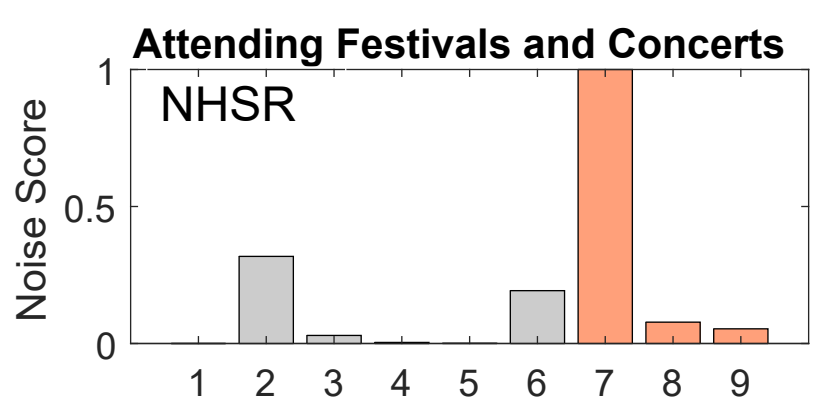
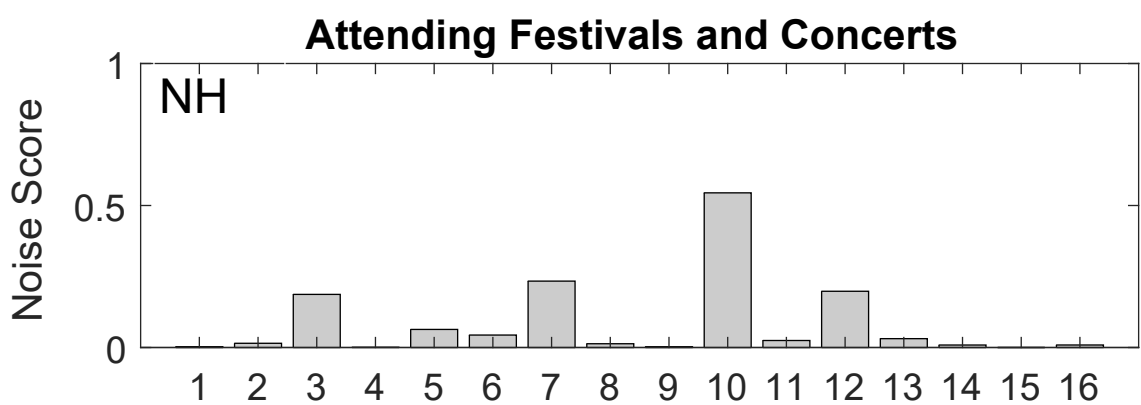
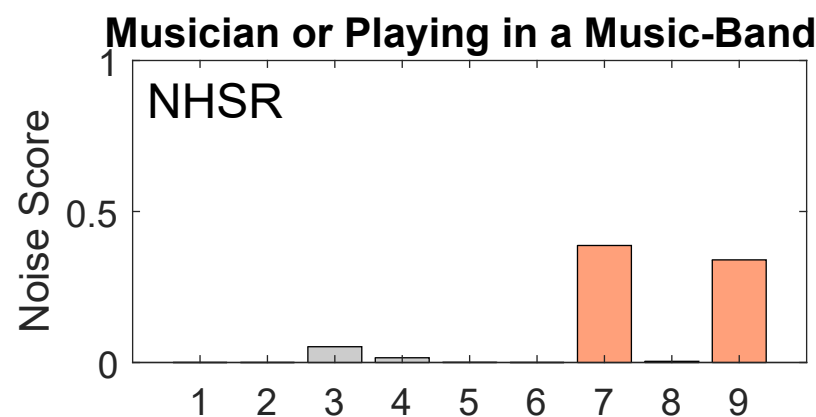
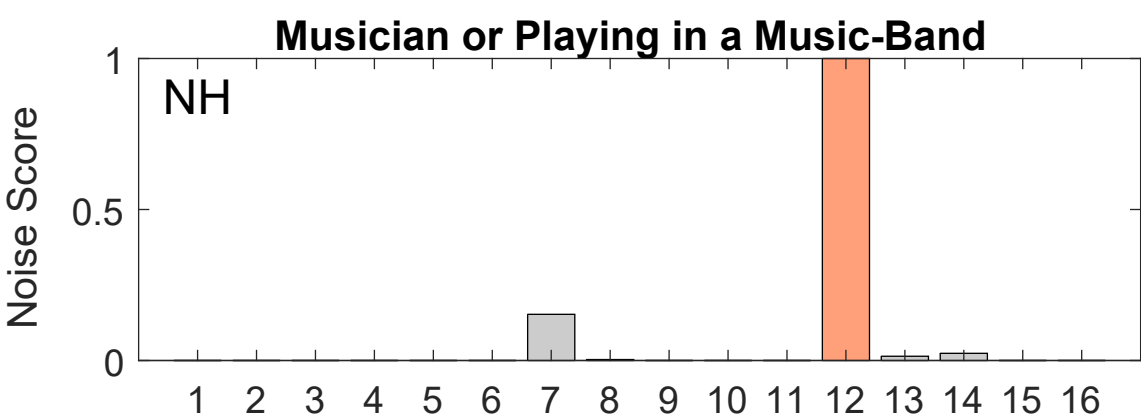
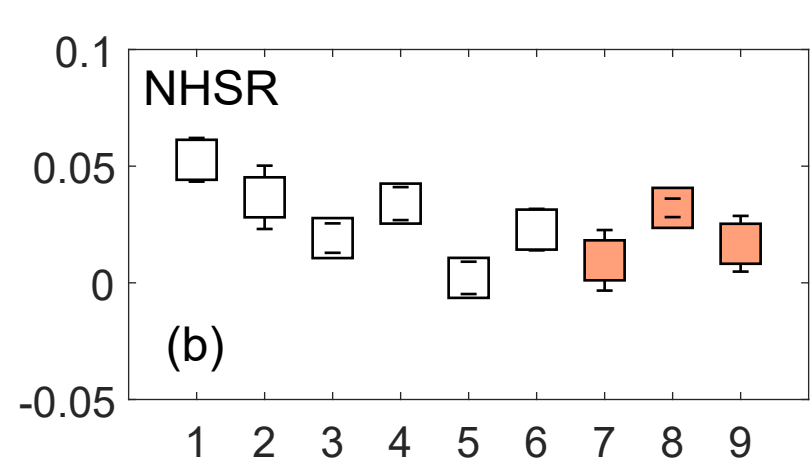
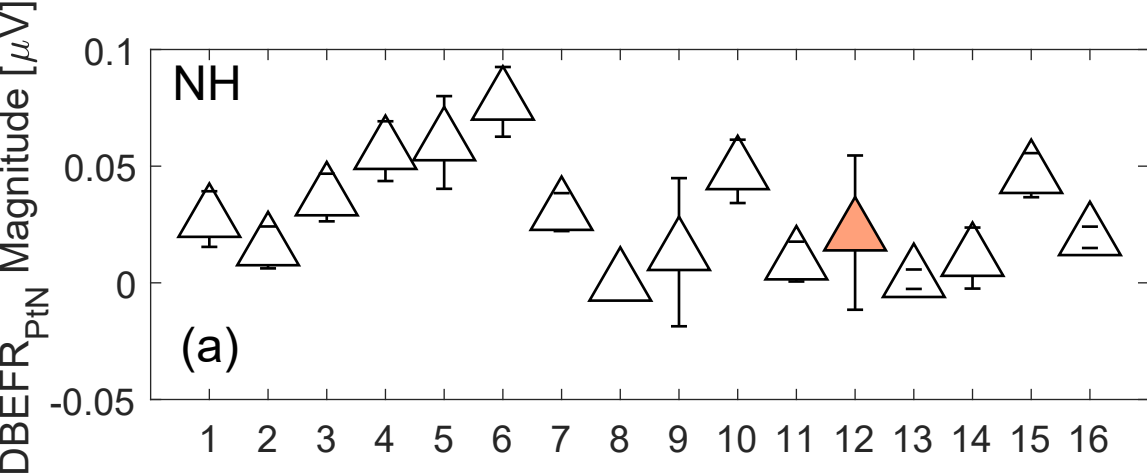




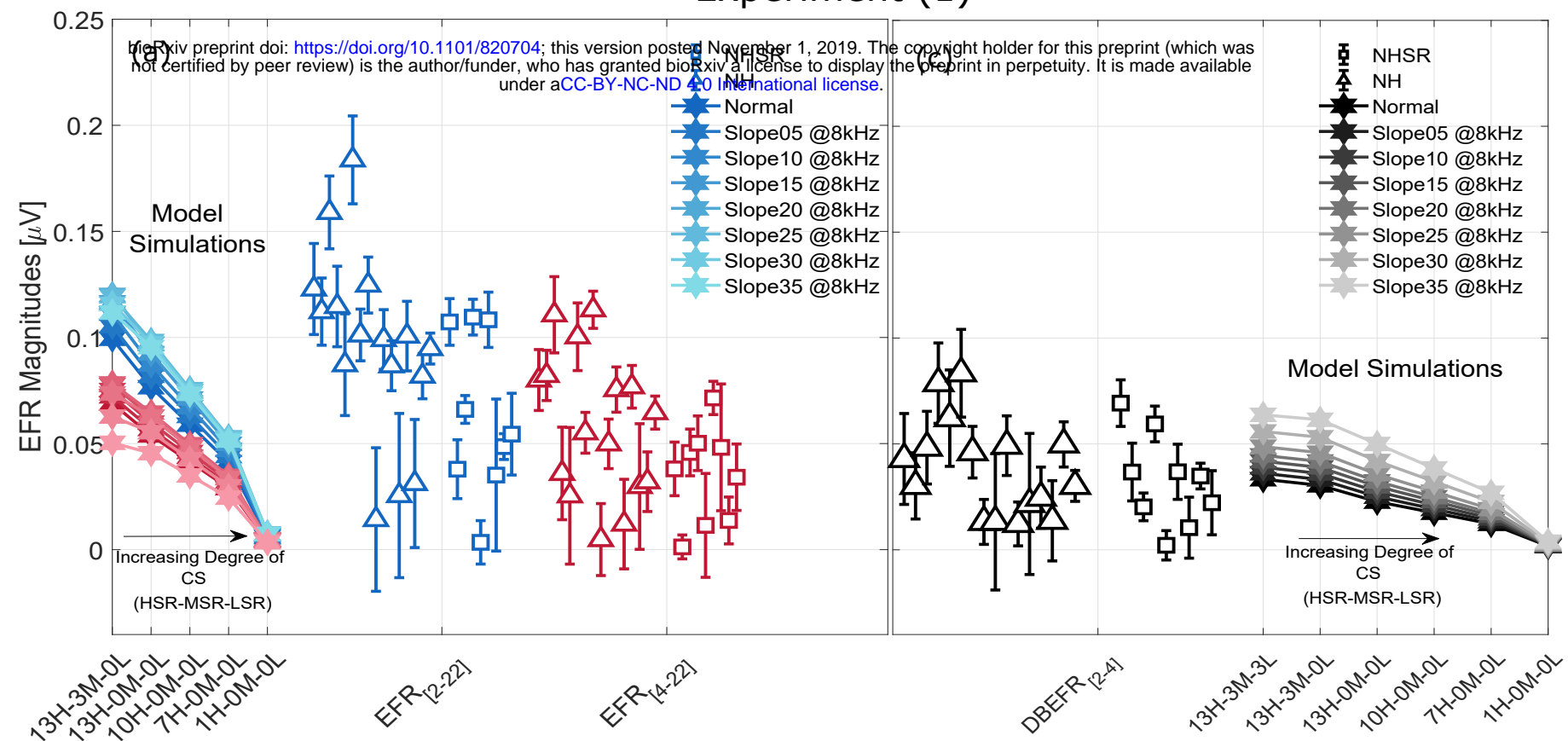








Experiment (1)



Experiment (2)

